

CHIRALITY VIOLATION IN THE QCD HIGH-ENERGY S-MATRIX*

Alan. R. White[†]

High Energy Physics Division
Argonne National Laboratory
9700 South Cass, IL 60439, USA.

Abstract

In a previous paper it has been shown that the infra-red divergence associated with the triangle graph axial anomaly can occur in triple-regge multi-reggeon interactions due to unphysical asymptotic triple discontinuities. In this paper an asymptotic discontinuity analysis is applied to high-order feynman diagrams to show that the anomaly exists in contributions to the triple-regge nine-reggeon interaction. This implies that the anomaly occurs in the interactions of reggeon states that have the quantum numbers of the anomaly current and establishes a direct connection with the well-known U(1) problem.

*Work supported by the U.S. Department of Energy, Division of High Energy Physics, Contracts W-31-109-ENG-38 and DEFG05-86-ER-40272

[†]arw@hep.anl.gov

1. INTRODUCTION

Perhaps the most important property of a non-abelian gauge theory is the existence of non-perturbative euclidean classical solutions with non-trivial topology. If the theory is quantized (in principle at least) via the euclidean path-integral, such solutions produce additional interactions that, even if it is not well understood how to evaluate them, are believed to modify properties of the theory significantly. In particular, the topological field configurations produce zero modes of the Dirac operator which[1] prevent the gauge-invariant separation of massless fermion fields into chiral (right- and left-handed) components that create particles and antiparticles in a well-defined way. As a result, the number of right- and left-handed Dirac particles is not separately conserved. The corresponding U(1) vector charge remains conserved, but the axial charge conservation that is present in perturbation theory is violated non-perturbatively, as allowed by the anomaly in the U(1) axial current. We expect, therefore, that quark chirality transitions will play an important role within the QCD bound-state S-Matrix. (It is well-known that such processes can generate a mass[2] for a bound-state with the quantum numbers of the η' .) Clearly, how such transitions contribute must be a major component of a complete non-perturbative definition of the massless theory.

In this paper we will provide evidence for a completely different argument that there should be non-conservation of the U(1) axial charge in the high-energy (multi-regge) QCD bound-state S-Matrix. This argument makes no mention of either the euclidean region, path-integral quantization, or zero modes. Rather it is part of a program which has gradually taken shape over the years[3, 4] and which we expect to carry out in detail in future papers. The aim of the program is to construct the massless, multiparticle, multi-regge S-Matrix starting from a spontaneously-broken theory in which gluons and quarks are massive, and regge behavior and the unitarity properties of reggeon diagrams are well-established perturbatively[5, 6]. The massless theory that is our ultimate goal is, of course, infra-red divergent and it is widely believed that even if the divergences could be handled systematically the large order behavior of the perturbation expansion is so bad that it can not be used (by itself) to define the theory. However, we plan to initially apply our construction to the case in which the gauge coupling does not increase in the infra-red region[‡] and the divergence of the perturbation series is reduced considerably. In addition, the multi-regge region may be a special situation. Because high-energy is involved, the S-Matrix should be close to perturbation theory while, because low momentum transfers are also involved, t -channel unitarity properties involving the physical spectrum must also be satisfied.

[‡]This requires an infra-red fixed point in the massless β -function which, in turn, is likely to require a special fermion content.

If it is possible to construct the multi-regge behavior of a weak-coupling, massless, theory from the essentially perturbative starting point of massive reggeon diagrams, without reference to the low-energy solution of the theory, then there must be some element that can produce the “non-perturbative” properties of confinement and chiral symmetry breaking in the spectrum. We expect that, in our construction, this will be the triangle anomaly “chirality violation” that we argued in [3] can occur[§] in certain reggeized gluon interactions due to a quark loop. In our future papers, we hope to demonstrate that a multi-regge S-Matrix with all the desired properties is obtained by combining perturbative multi-regge infra-red behavior with a treatment of the anomaly that clearly breaks the U(1) axial symmetry. As a prelude to the full program, therefore, we must first establish that the U(1) anomaly (and also the chiral flavor anomaly - which plays a crucial role in the chiral symmetry breaking) does indeed appear in the framework of multiparticle multi-regge behavior. Our focus in this paper will be on explaining in detail the origin of this phenomenon. Our hope is that this explanation will add considerably to the arguments that we have already given[3].

Reggeon diagrams contain reggeized gluon (or quark) propagators, reggeon interaction vertices, and external couplings to the scattering states, all of which are gauge invariant, even in perturbation theory. In general, many Feynman diagrams give contributions to a single reggeon diagram and, therefore, to a single reggeon interaction. In addition, a reggeon interaction vertex has a significance that goes beyond it’s perturbative description. As we will see, the essential “non-perturbative” element of the calculations we describe is the role played by unphysical asymptotic multiple discontinuities and the anomaly in contributions to reggeon interaction vertices that they give. The anomaly in such contributions can be non-perturbative in the sense that it can be present in a reggeon vertex but not necessarily produce an effect in a perturbative amplitude in which it is contained. This is because the structure of external couplings and additional symmetries of full reggeon diagrams can be sufficient to produce a cancelation. Indeed, we argued in [3] that when the scattering states are elementary quarks or gluons the anomaly always cancels in the full scattering amplitude. Conversely, we expect it to play a crucial role in the scattering of “non-perturbative” physical bound states.

Before enlarging further on the significance of unphysical asymptotic multiple discontinuities and the results of this paper, it will be helpful to briefly discuss the potential relationship between our work and the euclidean path-integral formalism. We note, first, that in Minkowski space the Dirac zero modes due to topological gauge fields are manifest[1] as the spectral flow of the eigenvalues of the corresponding (gauge-dependent) “Hamiltonian”. Since there is no complete non-perturbative

[§]We will discuss precisely what we mean by “chirality violation” and “the anomaly” in this context shortly.

Hamiltonian formalism for QCD, there is no well-developed understanding of what the general consequences of spectral flow might be. The common expectation is probably that such phenomena will be overwhelmed by strong-coupling effects of the kind usually assumed to be associated with confinement. However, in a massless theory in which the gauge coupling remains small in the infra-red region, we should not expect this to be the case. As a minimum, we anticipate that (in an appropriate background field) zero energy fermion states identified initially as a particle (presumably within a boundstate) can evolve with time into a filled vacuum state of the corresponding Dirac sea and, similarly, filled vacuum states can evolve into particles. (The existence of stable bound states and physical scattering processes in such an environment is surely far from trivial!)

The U(1) anomaly can be interpreted in terms of infra-red spectral flow as follows. Associated with the anomalous divergence equation, the massless axial-vector triangle graph has[7] an infra-red divergence that involves a zero four-momentum propagator. Both the “particle” and “antiparticle” poles of the propagator contribute to the divergence. The coupling at one end of the propagator can be viewed as the vertex for production of the particle while simultaneously (and symmetrically) that at the other end describes the production of the antiparticle. For the propagator to describe a physical zero momentum transition there must be spectral flow (due to a background gauge field) in that the production of the antiparticle (or the particle) must be counted as the absorption of a particle (antiparticle). In this case, the transition becomes a “chirality transition”. Consequently, in Minkowski space the U(1) divergence equation provides a connection between the topological structure of a background gauge field and the net infra-red “spectral flow” of zero momentum, massless, Dirac particle and antiparticle states.

In our analysis “spectral flow” is introduced by the appearance of the triangle graph infra-red divergence (referred to above as the “anomaly”) in reggeized gluon interactions. The triangle graph appears as an effective interaction generated by particular multi-gluon interactions due to a quark loop. There are no axial-vector currents in the QCD interaction but, as we already described in [3], multi-regge effective interactions can contain components of an axial-vector interaction. In sufficiently high order, interactions appear involving reggeon states with the quantum numbers of the anomaly (winding-number) current. Remarkably, perhaps, we will establish in this paper that it is interactions of this last kind that have the contributions from unphysical multiple discontinuities that we argued in [3] are necessary for the anomaly infra-red divergence to appear. As a result, the U(1) problem is clearly encountered. Indeed, we anticipate that the infra-red discussion we give is connected to “ultra-violet” problems (involving momenta flowing around the internal quark loop that are comparable in magnitude to the large external momenta) that reflect the usual relationship between infra-red and ultra-violet manifestations of the anomaly. We

would expect short-distance interactions of the winding number current to appear directly in this ultra-violet context. (It is, perhaps, unfortunate that the anomaly is a high-order, many gluon, phenomenon. However, this is to be expected if the anomaly current, containing a product of three gluon fields, has to be involved.)

We will call the basic process, in which a physical region zero momentum propagator contributes to a triangle graph divergence, a chirality transition and will refer to the general phenomenon as “chirality violation”, although we could equally well call it spectral flow[¶]. It will also be what we generically refer to as “the anomaly”, within our formalism. In this paper, as in [3], we will concentrate on the feynman diagram amplitudes that produce the anomaly in reggeon interactions and, apart from the brief description at the end of this Introduction, will not discuss the general program any further. In [3] we distinguished two methods for calculating multi-regge amplitudes - the direct calculation of diagrams in light-cone co-ordinates and the calculation of multiple asymptotic discontinuities with the subsequent use of an asymptotic dispersion relation. We emphasized that the direct calculational method is impractical for the problem we are discussing. This is because of the large number of diagrams that could contribute and because the complexity of the diagrams makes a full discussion of whether or not integration contours are truly trapped, in the asymptotic limits involved, very difficult. Consequently the asymptotic dispersion relation method has to be used.

The form of the asymptotic dispersion relation for a given multi-regge process is determined by the asymptotic multiple discontinuities that satisfy the Steinmann relation property that the discontinuities occur in non-overlapping invariant channels. Such discontinuities are explicitly reflected in the analytic structure of asymptotic amplitudes and, conversely, using the dispersion relation, amplitudes can be calculated directly from the discontinuities[6, 10]. The crucial feature of the high-order amplitudes that produce reggeon interactions containing the anomaly is the presence of unphysical multiple discontinuities that satisfy the Steinmann relation property. Such discontinuities are present only in complex (imaginary momentum) parts of the asymptotic region for more complicated many-particle multi-regge processes, the simplest of which is the full triple-regge region[11]. However, just because they are in non-overlapping channels these discontinuities can (and must) consistently appear in the asymptotic amplitudes that describe also the real physical region behavior.

The familiar amplitudes that appear in multi-regge production processes (such as those that contribute to the BFKL equation[5]) do not contain unphysical multiple discontinuities. Rather they contain only multiple discontinuities that are naturally

[¶]Neither description is strictly appropriate. Since we study only S-Matrix elements we can not define chirality via right and left-handed fields and since we do not have a hamiltonian we also can not define spectral flow in the normal manner. We also can not define the anomaly in terms of the divergence of an axial current although we can, as we discussed in [3], relate it to the violation of reggeon Ward identities that normally are a consequence of gauge invariance.

interpreted as due to a succession of physical region on-shell scattering processes[6]. (The necessity for a physical time-ordering of such processes then determines the absence of overlapping channel discontinuities.) Because the physical region multiple discontinuities involve only physical amplitudes and physical intermediate states, when they are calculated using the perturbative amplitudes of the massless theory, they can not contain chirality transitions associated with particle/antiparticle ambiguities. Therefore, when only production processes are involved (i.e. at what we might call the BFKL level of multi-regge theory) there is no possibility for “chirality violation”. In more elaborate scattering processes the unphysical multiple discontinuities appear and they may, a-priori, contain potential chirality transitions, even when calculated perturbatively. This is because the discontinuities involved may contain what, in a physical region, would be mixed combinations of forward-going particles and backward going antiparticles (“mixed α singularities”, in the language of S-Matrix Theory). Our purpose, in this paper, is to show that this phenomenon does occur and to demonstrate that, in the massless limit, the reggeon interactions associated with the asymptotic amplitudes can contain the anomaly and so, potentially, can produce physical region infra-red divergences.

In our previous paper studying triple-regge interactions[3] we already discussed why the anomaly could only appear in reggeized amplitudes containing unphysical triple discontinuities. In practise, however, we only studied (what appeared to be) the lowest-order relevant diagrams, i.e. those that contain two gluons in each t -channel. We isolated the physical momentum configuration within “maximally non-planar” diagrams that, in the massless (quark) limit, could potentially give an infra-red divergence associated with the anomaly, provided the appropriate on-shell propagators contribute to the asymptotic behavior. However, although they are maximally non-planar these diagrams do not have the complexity required to contain the unphysical triple discontinuities that, according to our method of analysis, would determine that these propagators do contribute. We noted, nevertheless, that the necessary discontinuities did appear to be present in the higher-order amplitudes that would give the reggeization of the gluons in the diagrams we studied. Therefore, we argued, the anomaly configurations in the lowest-order diagrams could be required as (generalized) real parts needed to accompany the higher-order unphysical triple discontinuities. Paradoxically, perhaps, we simultaneously suggested that there would be cancelations among diagrams such that the anomaly would survive only when reggeon states with the quantum numbers of the winding-number current are involved.

In this paper we will study the high-order reggeization diagrams in detail and will find that the situation is actually simpler than we suggested. The anomaly infra-red divergence is produced by a quark loop in which many propagators are on-shell and one propagator carries the zero momentum and energy that allows a chirality transition. The on-shell conditions have to be associated with a triple discontinuity in such a way that a triplet of the on-shell particles (each associated with a separate

discontinuity) are all quarks (or all antiquarks). It is straightforward to see that this “all quarks” requirement can not be satisfied by a physical discontinuity and that, in fact, it is very difficult to satisfy. Indeed, we find that the reggeization diagrams that we suggested in [3] might contain the anomaly actually do not satisfy the all-quarks requirement. As we proceed to higher orders we eventually find that this requirement is satisfied. However, a final requirement that the spin structure that generates the anomaly also be present, further restricts the triple discontinuities that can contribute. Eventually we arrive at (a small class of) diagrams that contain a triple discontinuity with all the right properties. However, this discontinuity is truly unphysical in that it occurs as a combination of three “asymptotic pseudothresholds” each of which contains particles, effectively, going in opposite time directions. The reggeon interactions produced are also of sufficiently high order that the minimum circumstances in which they can occur (between color zero reggeon states) is when each of the states involved carries the quantum numbers of the $U(1)$ anomaly current. Nevertheless, this establishes the essential result of this paper that the triangle anomaly does occur in reggeized gluon interactions extracted from unphysical multiple discontinuities and that the phenomenon we are discussing is indeed the $U(1)$ anomaly. The results of this paper also imply that the lower-order diagrams considered in [3], although valuable to discuss for illustrative processes, are essentially irrelevant.

In this paper we are satisfied to simply demonstrate that there are diagrams which generate a reggeon interaction in which the anomaly appears, and that the reggeon states involved have the quantum numbers of the anomaly current. We do not discuss whether there are cancelations that could occur. We postpone this for the following papers that will lay out the details of the construction of the bound-state S-Matrix alluded to above. For the moment we note only that triple-regge interactions of the kind we consider here will contribute generally to the vertices and interactions of the reggeon bound states that emerge and refer to the brief discussion in [3], and also the outline in [4], for more details. A brief, general, description of the anticipated construction is as follows.

We expect to obtain massless QCD from the massive theory in two stages. In the first stage, the (spontaneously-broken) gauge symmetry is restored to $SU(2)$. The $U(1)$ chiral symmetry is broken by the introduction of a “wee-parton” condensate with anomaly current quantum numbers in scattering reggeon bound states. Our expectation is that an anomaly infra-red divergence then appears and determines the “physical scattering amplitudes”. After the divergence is factorized off, the condensate self-consistently appears in all intermediate and final reggeon states. An essential ingredient will be to show[3] that if we regulate the anomaly ultra-violet divergences involved, the infra-red divergence gives a result that is independent of the regularization used. (Note that, by identifying, regulating, and organizing how chirality violation divergences produce reggeon states and scattering processes, we constrain

how, in the path-integral formalism, non-perturbative topological gauge fields must contribute to the massless theory. Indeed, if we succeed in our goals, we will implicitly determine how the spectral flow of the Dirac sea must contribute if a unitary high-energy S-Matrix is to be obtained.)

U(1) chirality violation appears within interactions of the pomeron and additional chirality violation, related to the anomaly in flavor current vertices, is responsible for the appearance of the pion and the “nucleon”. (At this stage, the nucleon (to be) is a chiral Goldstone boson, just like the pion.) The pomeron should be in a supercritical phase of Reggeon Field Theory and the spectrum of bound-states should have both SU(2) confinement and chiral symmetry breaking^{||}. In the second stage, the full gauge symmetry is to be restored by the randomization of the SU(2) condensate within SU(3). The randomization should correspond to a phase-transition within Reggeon Field Theory. We expect that the asymptotic freedom requirement that contact with perturbation theory remain at short distances determines that the theory must be right at the critical point associated with critical behavior for the pomeron[9].

Finally, we note that while we have not studied the issue in any detail, we believe that when the fermions involved are massive only the “ultra-violet anomaly” is present. As we remarked above, this will produce problems (for bound-state scattering amplitudes) in the (internal) momentum region of reggeon interactions where the momenta are of the order of, or larger, than the external regge limit momenta and effective interactions of the anomaly current should be directly involved. A-priori, we expect the presence of the anomaly, in this form, to lead to the violation of reggeon Ward identities and to increased power behavior asymptotically for the amplitudes in which it is contained. A consequent violation of unitarity bounds by potential bound-state amplitudes is therefore threatened and this is clearly where non-perturbative topological contributions could be crucial. Of course, if the anomaly produces infra-red divergent amplitudes in the massless theory, it could also imply that the reggeon diagram result for the asymptotic behavior is wrong and unitarity bounds could be threatened. However, the implication of the infra-red divergence structure we envision is that the divergences both select the physical states and can be absorbed into a redefinition of the states that leaves reggeon asymptotic behavior intact. Thus, as a matter of both principle and practicality we believe that the massless multi-regge amplitudes must be constructed first - by a procedure that regularizes the ultra-violet anomaly and allows the infra-red behavior to dominate. We also believe that it is the relative simplicity of the infra-red structure of the anomaly, together with the unitarity properties of reggeon diagrams and their relationship with Reggeon Field Theory, that will allow us to carry out such a procedure.

^{||}It is possible, if not likely, that the role of the Dirac sea in producing confinement in this context is related to that proposed by Gribov[8].

2. MULTIPLE DISCONTINUITIES AND THE STEINMANN RELATIONS.

The Steinmann relations originated in axiomatic field theory[12]. They (essentially) describe the restrictions that the time-ordering of interactions places on the combinations of intermediate states that can occur in a scattering process. For on-shell S-Matrix amplitudes their significance is most immediately appreciated in the approximation that we ignore higher-order Landau singularities and consider only the normal threshold branch points (and stable particle poles) that occur in individual channel invariants. The Steinmann relations then say that simultaneous thresholds (and/or poles) can not occur in overlapping channels. (Channels overlap if they contain a common subset of external particles.) As a result an N -point amplitude has at most $N - 3$ simultaneous cuts (or poles) in distinct invariants. The possible combinations of cuts can be described by tree diagrams with three-point vertices in which each internal line corresponds to a channel invariant in which there is a cut due to intermediate state thresholds - as illustrated in Fig. 2.1 for the 7-point amplitude.

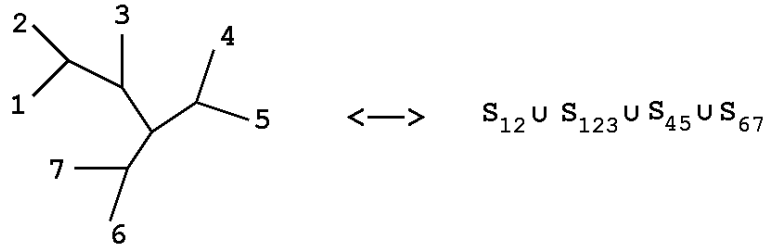


Fig. 2.1 A Tree Diagram Representing Simultaneous Invariant Cuts.

(As usual, $s_{12} = (P_1 + P_2)^2$, $s_{123} = (P_1 + P_2 + P_3)^2$, etc.) The set of all combinations of thresholds (and poles) allowed by the Steinmann relations is the basic singularity structure of all scattering amplitudes. The higher-order Landau singularities are believed[10] to emerge from the normal thresholds in a manner that for many purposes (including ours, as we discuss shortly,) makes them a secondary effect.

Conversely, the combination of cuts represented by a particular tree diagram can be directly associated with a set of physical scattering processes. As illustrated in Fig. 2.2, this is the set of all processes (involving all the external particles of the diagram as either ingoing or outgoing particles) in which it is kinematically possible for all of the internal lines to be replaced by physical multiparticle states**.

**We do not distinguish processes in which ingoing and outgoing particles are interchanged via CPT conjugation

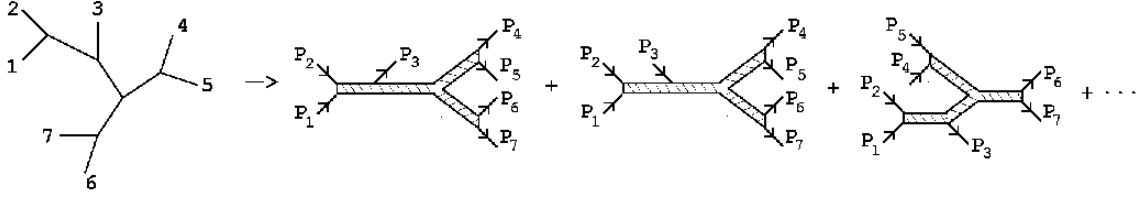


Fig. 2.2 Physical Scattering Processes Corresponding to Fig. 2.1.

The hatched segments represent physical intermediate states that, if they are all placed on shell, give (essentially) the associated multiple discontinuity.

The Steinmann relations play a fundamental role in multi-regge theory. It is possible to show[10] that in a physical multi-regge asymptotic region the analytic structure of scattering amplitudes can be treated as if only normal thresholds satisfying the Steinmann relations were present. In effect, higher-order Landau singularities are suppressed. This has the very important consequence that only the normal threshold cuts in individual channel invariants need be represented by multi-regge asymptotic formulae. Furthermore, if we consider only the multi-regge limits accessible in $2 \rightarrow M$ production processes, it can be shown that the maximal number $(M-1)$ of simultaneous thresholds is encountered asymptotically only in physical regions. This is a generalization of the cut-plane analyticity property familiar from elastic scattering.

If we consider the multi-regge regions of $M \rightarrow M'$ scattering amplitudes $(M, M' \geq 3)$ there is a significant change. To understand the point involved consider the simplest case of the tree diagram of Fig. 2.3. At first sight this diagram corresponds only to the $2 \rightarrow 4$ production processes shown.

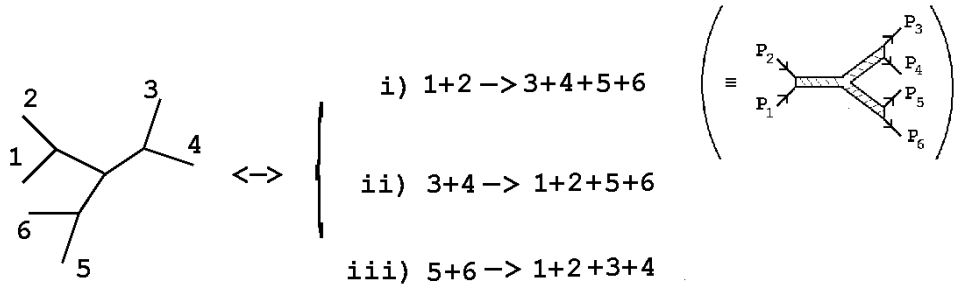


Fig. 2.3 A Tree Diagram and Corresponding Physical Scattering Processes.

The three distinct scattering processes are distinguished by different constraints on

the invariants, i.e.

$$\begin{aligned}
\text{i)} \quad & \sqrt{s_{12}} > \sqrt{s_{34}} + \sqrt{s_{56}} , \\
\text{ii)} \quad & \sqrt{s_{34}} > \sqrt{s_{12}} + \sqrt{s_{56}} , \\
\text{iii)} \quad & \sqrt{s_{56}} > \sqrt{s_{12}} + \sqrt{s_{34}}
\end{aligned}
\tag{2.1}$$

We can also regard the three processes involved as distinguished by the selection of one pair of particles as incoming, which then must have energy larger than the sum of the subenergies of the other two pairs, which are necessarily in the outgoing state.

We may wonder about the symmetric asymptotic region in which

$$\sqrt{s_{12}} \sim \sqrt{s_{34}} \sim \sqrt{s_{56}} \rightarrow \infty
\tag{2.2}$$

There are no physical scattering processes in this region. However, the three processes of (2.1) are described by the same (analytically continued) amplitude and so analytic continuation from each of the physical regions implies that such cuts must be present. It is, perhaps, natural that a triple discontinuity should exist that is symmetric with respect to the three processes of Fig. 2.3. Apparently, though, the symmetry requirement could only be satisfied if all the external particles are in the final, or initial, state. However, as we discuss further in Sections 4 and 5, if we allow particles to carry complex momenta, a positive value for a two-particle energy invariant can be achieved by a combination of an “incoming” and an “outgoing” particle in that they carry opposite sign, but imaginary, energies. Therefore, in the symmetric region it is possible for the three cuts of Fig. 2.3 to be present if each is associated with such a combination. We will show in the following that there are unphysical processes (with imaginary momenta) in this region that do produce a triple discontinuity of this kind and we will refer to it as an “unphysical triple discontinuity”.

Because the external particles for each cut are both ingoing and outgoing, intermediate states can also be produced that involve such combinations. As a result, the triple discontinuity can contain the “particle - antiparticle” transitions that ultimately provide the massless chirality transitions that we are looking for. Moreover, since the complex momentum part of (2.2) is contained in the triple-regge asymptotic region, the triple discontinuity must be present in triple-regge asymptotic formulae. This is possible just because this combination of cuts has the Steinmann property. Moreover, because of the potential for chirality violation, it is a natural context in which to see the anomaly appear. The importance of the triple-regge region is that it is the simplest multi-regge limit in which the vertices appear that provide the couplings of bound-state regge poles such as the pomeron or the pion. For higher-point $M \rightarrow M'$ amplitudes there is a wide range of unphysical multiple discontinuities satisfying the Steinmann relations. Bound-state scattering amplitudes can thus appear in which the anomaly is a crucial element.

3. THE PHYSICAL REGION ANOMALY AND THE TRIPLE-REGGE DISPERSION RELATION

In our previous paper[3] we studied the full triple-regge limit[11] of three-to-three quark scattering. If we denote the initial momenta as P_i , $i = 1, 2, 3$, and the final momenta as $-P_i' = P_i + Q_i$, $i = 1, 2, 3$, the triple-regge limit can be realized, within the physical region, by taking each of P_1 , P_2 and P_3 large along distinct light-cones, with the momentum transfers Q_1, Q_2 and Q_3 kept finite, i.e.

$$\begin{aligned}
 P_1 \rightarrow P_{1+} &= (p_1, p_1, 0, 0), \quad p_1 \rightarrow \infty & q_1 = Q_1/2 &\rightarrow (\hat{q}_1, \hat{q}_1, q_{12}, q_{13}) \\
 P_2 \rightarrow P_{2+} &= (p_2, 0, p_2, 0), \quad p_2 \rightarrow \infty & q_2 = Q_2/2 &\rightarrow (\hat{q}_2, q_{21}, \hat{q}_2, q_{23}) \\
 P_3 \rightarrow P_{3+} &= (p_3, 0, 0, p_3), \quad p_3 \rightarrow \infty & q_3 = Q_3/2 &\rightarrow (\hat{q}_3, q_{31}, q_{32}, \hat{q}_3)
 \end{aligned} \tag{3.1}$$

Momentum conservation gives a total of five independent q variables which, along with p_1, p_2 and p_3 , give the necessary eight variables. The definition of the triple-regge limit in terms of angular variables is given in [3]. For our present purposes the above definition in terms of momenta will be sufficient. This will allow us to avoid the extra complication of defining helicity angles, helicity-pole limits etc. It will be important that the asymptotic behavior involved must hold also for all complex values of the large momenta, including the additional physical regions reached by reversing the signs of the p_i .

In [3] we also studied feynman diagrams that contain a closed quark loop and generate triple-regge reggeized gluon interactions containing the loop. We considered the lowest-order amplitudes in which the anomaly could potentially appear and, in particular, studied maximally non-planar diagrams of the kind shown in Fig. 3.1(a).

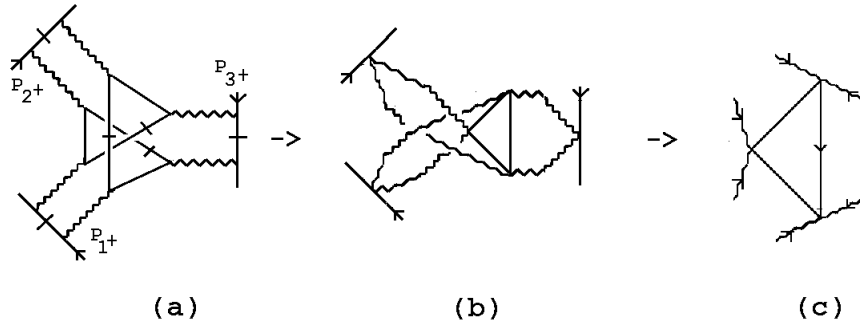


Fig. 3.1 A maximally non-planar diagram and rhe triangle diagram reggeon interaction prouced.

(As usual, the solid and wavy lines respectively represent a quark and a gluon. We

have reversed the direction of P_3 relative to the notation of [3] in order to have a completely symmetric notation.) The leading asymptotic contributions come from regions of gluon loop integrations where some of the propagators in the quark loop and the scattering quark systems are on-shell. We discuss the determination of which propagators can be on-shell below. For the moment we consider the possibility, discussed at length in [3], that the on-shell lines are those that are hatched in Fig. 3.1(a). We will eventually conclude that this combination of on-shell propagators can not produce a reggeon interaction with a physical region anomaly divergence, even though it does produce a triangle diagram interaction. As we will see, the issue is not just which propagators are placed on-shell but also which pole (“particle” or “antiparticle”) is involved. (As the discussion in the previous Section suggested, for the unphysical discontinuities, with which we will ultimately be concerned, the answer to this question is not necessarily unambiguous.) In the following we initially ignore this subtlety. As it emerges in our discussion it will become clear that it is a vital part of the search for further diagrams which do produce an interaction containing the anomaly.

If the hatched on-shell propagators are used to carry out light-like longitudinal momentum integrations the integrals over gluon loop momenta reduce to two-dimensional “transverse” integrals over spacelike momenta, as illustrated by Fig. 3.1(b). The transverse plane (and orthogonal light-like momenta) can, in general, be chosen differently in each t -channel. If $Q_{i\perp}$ is the projection of Q_i on the corresponding transverse plane, the leading asymptotic contribution then has the form

$$P_{1+} P_{2+} P_{3+} \prod_{i=1}^3 \int \frac{d^2 k_{i1} d^2 k_{i2}}{k_{i1}^2 k_{i2}^2} \delta^2(Q_{i\perp} - k_{i1} - k_{i2}) G_i^2(k_{i1}, k_{i2}, \dots) \times R^6(Q_1, Q_2, Q_3, k_{11}, k_{12}, \dots) \quad (3.2)$$

where $R^6(Q_1, Q_2, Q_3, k_{11}, k_{12}, \dots)$ can be identified with the “reduced”, or “contracted”, feynman diagram of Fig. 3.1(c). If we write

$$k_{i1} = q_i + k_i, \quad k_{i2} = q_i - k_i, \quad (3.3)$$

then (with a particular choice[3] of transverse planes)

$$R^6(q_1, q_2, q_3, k_1, k_2, k_3) = \int d^4 k \frac{Tr\{\gamma_5 \gamma^{-, -, +}(\not{k} + \not{k}_1 + \not{q}_2 + \not{k}_3) \gamma_5 \gamma^{-, -, -} \not{k} \gamma_5 \gamma^{-, -, -}(\not{k} - \not{k}_2 + \not{q}_1 + \not{k}_3)\}}{(k + k_1 + q_2 + k_3)^2 k^2 (k - k_2 + q_1 + k_3)^2} + \dots \quad (3.4)$$

where

$$\gamma^{\pm, \pm, \pm} = \gamma^\mu \cdot n_\mu^{\pm, \pm, \pm}, \quad n^{\pm, \pm, \pm\mu} = (1, \pm 1, \pm 1, \pm 1) \quad (3.5)$$

The contributions to R not shown explicitly in (3.4) do not have a γ_5 at all three vertices of the triangle diagram. The particular γ -matrix projections appearing depend on the choice of transverse co-ordinates. If the anomaly is present in R , however, we expect it to be independent of this choice. We should emphasize that while we have written (3.4) as a function of four-dimensional momenta, the k_i are restricted to be two-dimensional spacelike momenta (plus longitudinal components determined by the mass-shell conditions for the on-shell quarks) and the q_i have the restricted form given by (3.1). These restrictions plays a crucial role in determining whether the anomaly can occur in a physical region reggeon interaction.

A reggeon diagram amplitude that represents right-hand cuts in the unphysical triplet $\{s_{13'}, s_{32'}, s_{21'}\}$ and has two reggeons in each t -channel, each with trajectory $\alpha(t) = 1 + O(g^2)$, has the form[3]

$$\begin{aligned}
& \prod_i \int \frac{d^2 k_i}{\sin \pi \alpha(k_i^2) \sin \pi \alpha((Q_i - k_i)^2)} \beta(k_1, k_2, k_3, Q_1, Q_2, Q_3) \\
& \left[(s_{13'})^{[\alpha(k_1^2) + \alpha((Q_1 - k_1)^2) + \alpha(k_3^2) + \alpha((Q_3 - k_3)^2) - \alpha(k_2^2) - \alpha((Q_2 - k_2)^2) - 1]/2} \right. \\
& \quad (s_{32'})^{[\alpha(k_3^2) + \alpha((Q_3 - k_3)^2) + \alpha(k_2^2) + \alpha((Q_2 - k_2)^2) - \alpha(k_1^2) - \alpha((Q_1 - k_1)^2) - 1]/2} \\
& \quad \left. (s_{21'})^{[\alpha(k_1^2) + \alpha((Q_1 - k_1)^2) + \alpha(k_2^2) + \alpha((Q_2 - k_2)^2) - \alpha(k_3^2) - \alpha((Q_3 - k_3)^2) - 1]/2} \right] / \quad (3.6) \\
& \left[\left[\sin \frac{\pi}{2} [\alpha(k_1^2) + \alpha((Q_1 - k_1)^2) + \alpha(k_3^2) + \alpha((Q_3 - k_3)^2) - \alpha(k_2^2) - \alpha((Q_2 - k_2)^2)] \right] \right. \\
& \quad \sin \frac{\pi}{2} [\alpha(k_3^2) + \alpha((Q_3 - k_3)^2) + \alpha(k_2^2) + \alpha((Q_2 - k_2)^2) - \alpha(k_1^2) - \alpha((Q_1 - k_1)^2)] \\
& \quad \left. \sin \frac{\pi}{2} [\alpha(k_1^2) + \alpha((Q_1 - k_1)^2) + \alpha(k_2^2) + \alpha((Q_2 - k_2)^2) - \alpha(k_3^2) - \alpha((Q_3 - k_3)^2)] \right] \\
& \sim_{g^2 \rightarrow 0} (s_{13'})^{1/2} (s_{32'})^{1/2} (s_{21'})^{1/2} \prod_i \int \frac{d^2 k_i}{k_i^2 (Q_i - k_i)^2} \beta(k_1, k_2, k_3, Q_1, Q_2, Q_3) \quad (3.7)
\end{aligned}$$

Taking the triple discontinuity in $s_{13'}$, $s_{32'}$ and $s_{21'}$ removes the poles due to the sine factors in the square bracket, but leaves the $g^2 \rightarrow 0$ limit unchanged. Since the triple discontinuity is unphysical and of the kind discussed in the previous Section, according to the discussion in [3], the ‘‘six-reggeon interaction vertex’’ $\beta(k_1, k_2, k_3, Q_1, Q_2, Q_3)$ could contain the anomaly.

Writing

$$P_{1+} P_{2+} P_{3+} \equiv (s_{13'})^{1/2} (s_{32'})^{1/2} (s_{21'})^{1/2} \quad (3.8)$$

and comparing with (3.7) we see that (3.2) could be identified as a lowest-order contribution to such a reggeon diagram amplitude if the reduced feynman diagram

amplitude of Fig. 3.1(c) is identified as a reggeon vertex, i.e.

$$R^6(Q_1, Q_2, Q_3, k_1, Q_1 - k_1, \dots) \equiv \beta(k_1, k_2, k_3, Q_1, Q_2, Q_3) \quad (3.9)$$

Therefore, if (3.2) does represent a contribution to the asymptotic behavior of the feynman diagram in Fig. 3.1(a) it could contribute to a triple-regge amplitude of the form of (3.6). Note that while the right-side of (3.8) clearly has a triple discontinuity in $\{s_{13'}, s_{32'}, s_{21'}\}$, the left-side does not. The equivalence of the two sides is only determined if higher-order terms in (3.6) appear and add to (3.2) in the appropriate manner. Such terms are contributed by what we refer to as reggeization diagrams, both in the Introduction and in the following.

As we have emphasized, the amplitude (3.4) representing Fig. 3.1(c) is the full four-dimensional triangle diagram amplitude except that special γ -matrices appear at the vertices and only combinations of (essentially) two-dimensional transverse momenta flow through the diagram. As discussed in [3], the γ -matrix couplings are appropriate to produce the anomaly but whether the necessary momentum configuration can occur within a physical region and provide a physical region inra-red divergence is a non-trivial and subtle question that depends crucially on the choice of propagator poles used to put lines on-shell, as we now describe.

The divergence of the (massless) triangle diagram occurs[7, 3] when a single light-like momentum flows through the diagram and all other momenta are spacelike and scaled to zero. Such a momentum configuration for the reggeon interaction R appears to be (essentially uniquely) realized by that of the full feynman diagram shown in Fig. 3.2(a).

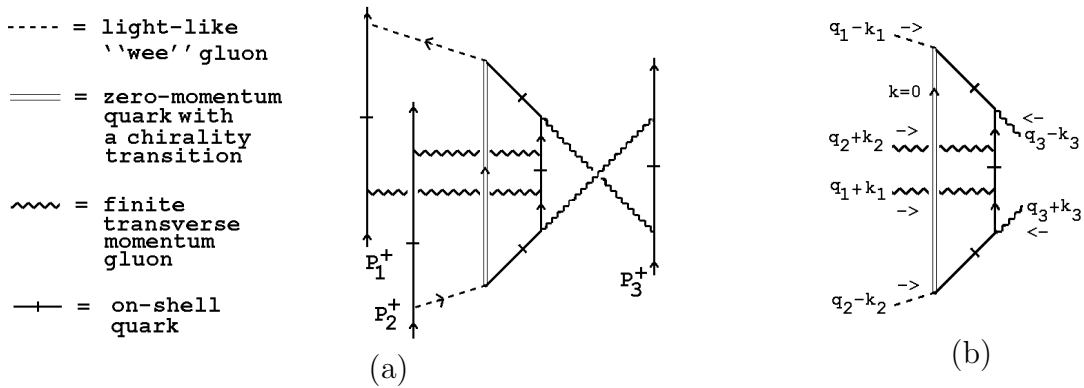


Fig. 3.2 The basic anomaly process.

If we label the momenta entering the reggeon interaction as in Fig. 3.2(b), an explicit

configuration for Fig. 3.2(a) is

$$q_1 - k_1 = (2l, 2l, 0, 0) , \quad q_2 - k_2 = (-2l, 0, -2l, 0) \quad (3.10)$$

together with

$$\hat{q}_1 = -\hat{q}_2 = l \quad q_{13} = -q_{23} \quad q_{12} = q_{21} = 0 \quad (3.11)$$

This determines k_1 and k_2 and also gives

$$q_3 = -(q_1 + q_2) = (0, -l, l, 0) \quad (3.12)$$

If we then take

$$k_3 = l(0, 1 - 2 \cos \theta , 1 - 2 \sin \theta , 0) \quad (3.13)$$

the light-cone momentum

$$- 2l(1, \cos \theta, \sin \theta, 0) \quad (3.14)$$

flows along the two vertical non-hatched lines in Fig. 3.2(b). It is straightforward to check that all three of the hatched lines are on mass-shell. If spacelike momenta of $O(q)$ are added to the momentum configuration (3.10)-(3.14) and the limit $q \rightarrow 0$ is taken the presence of the anomaly divergence will lead to the behavior

$$R^6(l, \theta, q) \underset{q \rightarrow 0}{\sim} \frac{(1 - \cos \theta - \sin \theta)^2 l^2}{q} \quad (3.15)$$

Apart from the reversal of direction for P_3 , the process represented by Fig. 3.2(a) is what we called “the basic anomaly process” in [3]. The scattering should be thought of as taking place with the time axis vertical on the page. The space axes are not, of course, represented accurately since each of the external quarks is traveling along orthogonal directions. The dashed lines indicate light-like (“wee parton”) gluons with finite momenta parallel to the incoming/outgoing quark that they are emitted/absorbed by. A zero-momentum quark (indicated by the open line) is emitted by the incoming wee-parton gluon and is absorbed by the outgoing wee-parton gluon. The first and last gluon interactions of the antiquark rotate it’s incoming/outgoing lightlike momentum to/from the triangle light-like momentum associated with the infra-red divergence. The two intermediate gluons carry equal but opposite transverse momenta. Their combination provides a forward scattering of the antiquark that, most importantly, includes a spin flip (the momentum factor for which reduces what would be a $1/q^2$ factor in (3.15) to $1/q$).

The zero momentum quark is produced by one wee gluon and absorbed by the other, allowing the chirality transition produced by the anomaly to compensate for the spin flip of the antiquark. Note, however, that when the wee gluons are massless, the scattering process represented by Fig. 3.2 is physical only when the quark and

antiquark involved are also massless. In addition, as we noted in the Introduction, the anomaly infra-red divergence involves both poles of the zero momentum quark propagator. According to the helicity analysis of [7] the vertices coupling to the propagator should be symmetrically interpreted as describing either the simultaneous production of the two states in the propagator or their simultaneous absorption. Therefore, if (the infra-red divergence analysis that we ultimately employ to define physical states and amplitudes should require that) we interpret the massless scattering as entering the physical region with the time ordering implied by Fig. 3.2, we are implicitly assuming the presence of a non-perturbative background gauge field. The background field would be needed to produce the necessary spectral flow at one vertex that is required to interpret the process as a chirality transition.

While the mass-shell conditions are indeed satisfied by (3.10)-(3.14), we must now discuss the important subtlety as to which propagator pole is chosen. With the momenta given by (3.10)-(3.14), the energy component of each of the three hatched lines in Fig. 3.2(b) has the same sign. Since the exchanged gluons carry only spacelike momenta, it is clear that this must be the case. Equivalently, the on-shell states in the loop must be treated symmetrically in that, if the zero momentum state is an antiquark (quark), all hatched lines must be quarks (antiquarks). We refer to this as the “all quarks requirement”. As we already remarked on in the Introduction, and as is discussed at length in [3], the only practicable calculational method to determine whether a given combination of on-shell lines contributes to the triple-regge behavior (after all diagrams are added) is the dispersion relation method that we outline very briefly below. In this approach all on-shell lines in a reggeon interaction result directly from the taking of a triple asymptotic discontinuity. “Real part” interactions with the same on-shell lines may be generated when the full dispersion relation is written or, equivalently, multi-regge theory is used[3] to convert the triple discontinuity to a full amplitude.

In fact, the “all quarks requirement” is (as we shall see from the examples we discuss below) very difficult to obtain in a reggeon interaction derived from a multiple discontinuity. We believe, however, that it is an essential requirement for a reggeon interaction to contain a physical region divergence produced by the anomaly, i.e. some variant of the “basic anomaly process” must be involved. We recognized in [3] that the necessary triple discontinuity is not present in the diagram of Fig. 3.1 but we suggested that nevertheless it may be present in the higher-order reggeization diagrams that produce the reggeization of the gluons and so the basic anomaly process of Fig. 3.2 may be required as a real part interaction (via the equivalence (3.8)). In fact, we will show in the remaining part of this paper that this is not the case. Instead, to satisfy the all quarks requirement, there must be at least two wee gluons (instead of one) either emitted, or absorbed, in the basic anomaly process. Ultimately this implies that reggeon interactions with the quantum numbers of the winding number current must be involved. As we emphasized in the Introduction (and also discussed in [3])

we do not expect the anomaly divergence to be present in the scattering of elementary quarks and/or gluons after all diagrams are summed. Rather, as we briefly comment on in Section 6, we expect it to be present when the basic process is generalized to describe the scattering of the particular multi-regge states that ultimately form bound states. The corresponding G_i will then appear in a generalization of (3.2) and the wee partons involved will be a crucial characteristic of scattering states. Also the chirality transitions produced (and the implicit spectral flow) will be an essential part of scattering processes.

In general, an asymptotic dispersion relation[10] gives the leading multi-regge behavior of an amplitude as a sum over multiple discontinuity contributions allowed by the Steinmann relations. For the particular case (described in detail in [3]) of the triple-regge behavior of a six-point amplitude we can write

$$M_6(P_1, P_2, P_3, Q_1, Q_2, Q_3) = \sum_{\mathcal{C}} M_6^{\mathcal{C}}(P_1, P_2, P_3, Q_1, Q_2, Q_3) + M_6^0, \quad (3.16)$$

where M_6^0 contains all non-leading triple-regge behavior, double-regge behavior, etc. and the sum is over all triplets \mathcal{C} of asymptotic cuts in non-overlapping (large) invariants. For each triplet \mathcal{C} , say $\mathcal{C} = (s_1, s_2, s_3)$, we can write

$$M_6^{\mathcal{C}}(P_1, P_2, P_3, Q_1, Q_2, Q_3) = \frac{1}{(2\pi i)^3} \int ds'_1 ds'_2 ds'_3 \frac{\Delta^{\mathcal{C}}}{(s'_1 - s_1)(s'_2 - s_2)(s'_3 - s_3)} \quad (3.17)$$

where $\Delta^{\mathcal{C}}$ is the triple discontinuity.

The triple discontinuities are of three kinds corresponding to the three tree diagrams of Fig. 3.3. There are 24 corresponding to Fig. 3.3(a), 12 corresponding to Fig. 3.3(b), and 12 of the Fig. 3.3(c) kind - including those described by Fig. 2.3. Those of Fig. 3.3(a) and (b), occur in the physical regions, while those corresponding to Fig. 3.3(c) are all unphysical triple discontinuities of the kind discussed in the last Section.

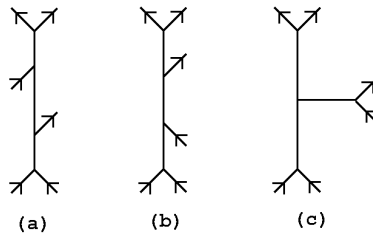


Fig. 3.3 Tree Diagrams for triple discontinuities.

As we discussed in [3], the diagram of Fig. 3.1(a) has physical region triple discontinuities of both the Fig. 3.3(a) and (b) kinds, although neither gives leading

triple-regge behavior. Unphysical discontinuities are more complicated to discuss. If the usual cutting rules hold, the diagram of Fig. 3.1(a) has no asymptotic triple discontinuities corresponding to Fig. 3.3(c), but rather has only double discontinuities. To see this, consider cutting the diagram as in Fig. 3.4, superficially giving an $\{s_{13'}, s_{32'}, s_{21'}\}$ triple discontinuity.

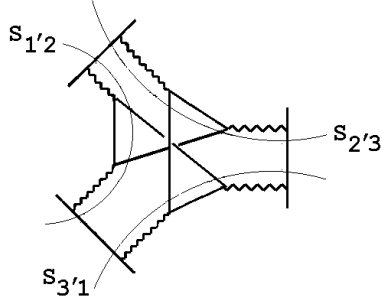


Fig. 3.4 An unphysical triple discontinuity?

In fact, taking any double discontinuity clearly cuts all the available lines, implying that there is no independent third discontinuity that can be taken.

It is not clear a-priori that the cutting rules do apply to unphysical discontinuities. However, we will show directly in Section 5 that there is no symmetric triple discontinuity present (giving the desired common energy component sign) in the diagram of Fig. 3.1. Therefore, as we described above, whether there is an anomaly contribution from diagrams of this kind depends on whether the necessary triple discontinuities are present when reggeization effects appear. In [3] we noted only that such discontinuities appeared to be present in reggeization diagrams but did not discuss the structure of such diagrams in any detail.

As an example of a diagram that should produce reggeization, consider that shown in Fig. 3.5

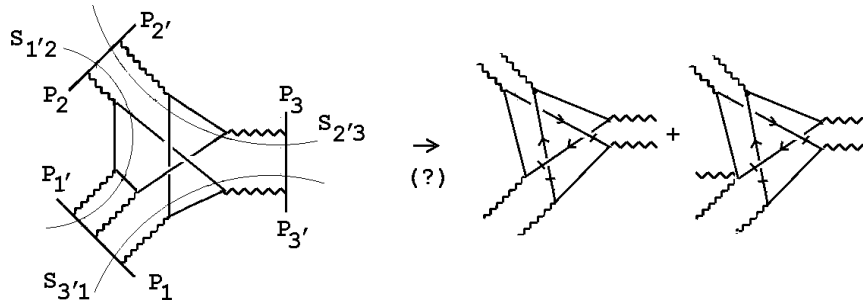


Fig. 3.5 A diagram with an unphysical triple discontinuity.

in which one of the gluons in the diagram of Fig. 3.4 is replaced by two-gluon exchange - potentially giving the one-loop contribution to the trajectory function of the original gluon. The thin lines again indicate how an unphysical $\{s_{13'}, s_{32'}, s_{21'}\}$ discontinuity would be taken. In such a contribution the corresponding six reggeon interaction, together with a remnant seven reggeon interaction, would be generated by putting the cut lines on-shell. The discontinuity is clearly not symmetric and, in addition, if the particles put on-shell by a discontinuity must be either all “incoming” or all “outgoing” (this is the “ $+\alpha$ ” condition that is part of the normal cutting rules) then the energy components of the on-shell lines in the quark loop (apart from that potentially giving the reggeization contribution) can not have the common sign required for the anomaly. This is because both the $s_{2'3}$ and $s_{3'1}$ cuts involve two of the relevant quark loop lines which must, therefore, be either incoming or outgoing quark/antiquark pairs. This requirement then eliminates the possibility that such lines are all antiquarks, or all quarks.

In the next Section we will confirm by direct calculation that the diagram of Fig. 3.5 does not have the triple discontinuity needed to give the anomaly. Consequently, the reggeon interactions generated do not contain the anomaly. Although a more complete analysis of all diagrams should be given, this essentially determines that the anomaly process of Fig. 3.2 is not generated as a “real part interaction” when higher-order reggeization effects are included.

To obtain a symmetric triple discontinuity in which the normal cutting rules could potentially give the anomaly amplitude associated with Fig. 3.2 , we consider the high-order diagram shown in Fig. 3.6(a)

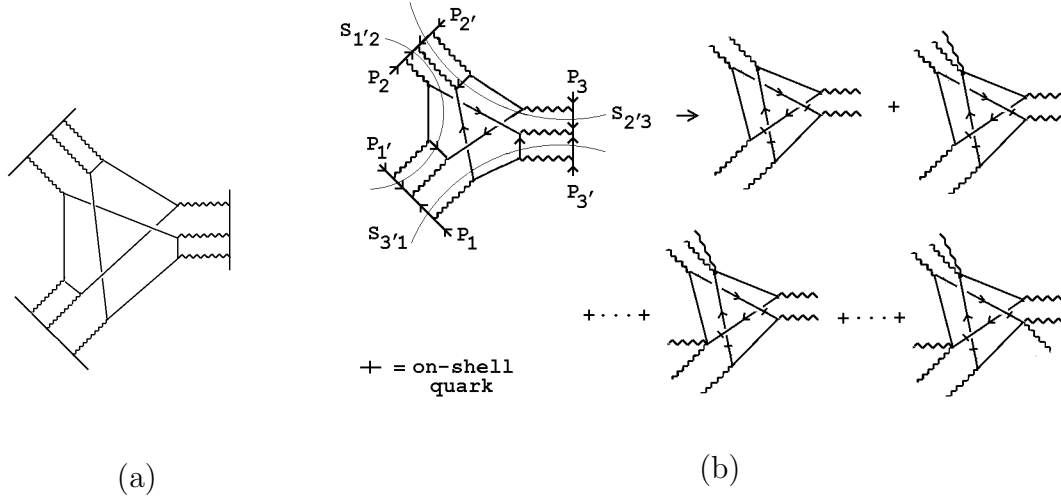


Fig. 3.6 (a) A diagram with a symmetric unphysical triple discontinuity
(b) expected reggeon interactions.

in which there are three gluons in each t -channel. A triple discontinuity in $\{s_{1'2}, s_{2'3}, s_{3'1}\}$ is obtained by cutting the diagram as indicated in Fig. 3.6(b). The closed loops involving two-gluon exchange could give both one loop contributions to the corresponding one reggeon trajectory function and the leading contribution of a two reggeon state. A-priori, therefore, we expect the diagram to contribute to the six-, seven-, eight- and nine-reggeon interaction as illustrated. Since the triple discontinuity is manifestly symmetric we again might expect the anomaly to appear in the six-reggeon interaction, just as anticipated by the lower-order amplitude of Fig. 3.1(a).

For consistency with our previous discussion, the anomaly should not (and does not) appear quite so simply. As will be clear after we carry out the explicit evaluation of asymptotic discontinuities in Section 5, the triple discontinuity of Fig. 3.6(b) requires a particular routing of the internal loop momenta. For this routing the numerators of the cut quark propagators do not give the combination of γ_5 interactions needed for the anomaly. In fact, the anomaly does occur within a reggeon interaction generated by the diagram of Fig. 3.6(a) but only when the unphysical discontinuities are actually taken as shown in Fig. 3.7. It then occurs in the nine-reggeon interaction obtained, as illustrated, by putting lines on-shell.

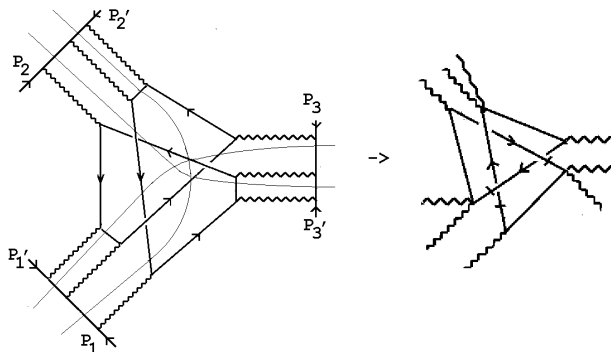


Fig. 3.7 Another cutting of Fig. 3.6(a).

Note that the discontinuity lines in Fig. 3.7 cross each other. This is possible because the particles contributing to each discontinuity do not all have the same time direction. To evaluate a multiple discontinuity of this kind we must develop direct methods to compute asymptotic discontinuities.

In the reggeon interaction of Fig. 3.7 there are three reggeons in each t -channel and each reggeon state is “vector-like” in that it has (close to) unit angular momentum and appears in odd-signature amplitudes. As discussed in [3], to avoid cancelation of the anomaly by transverse momentum integrations each reggeon state should have abnormal parity. Therefore, according to the above discussion, the simplest interaction in which the anomaly could appear is the nine-reggeon interaction in which each reggeon state is vectorlike, composed of (at least) three gluons, and has abnormal

parity. If, in addition, each reggeon state has zero color then all three states carry anomaly current quantum numbers. It is surely remarkable that we are led directly to the anomaly current by looking for the anomaly within reggeon interactions.

In fact, the analyticity properties of amplitudes require [3] that the anomaly appears only when signature conservation is also satisfied, which it is not if all three reggeon states carry odd signature. Therefore, to avoid cancelation when further diagrams are added, an additional (reggeized) gluon must be present in one t -channel. This gives only a relatively trivial modification of Fig. 3.7 and the analysis that follows. In this paper, we are not interested in determining when the anomaly ultimately survives after all diagrams are summed. We are satisfied just to find diagrams in which our asymptotic discontinuity analysis determines that the anomaly is definitively present in the extracted reggeon interaction. This already requires that we go to the complexity of Fig. 3.7.

4. LIGHT-CONE ANALYSIS OF ASYMPTOTIC DISCONTINUITIES

In the next Section we will analyse triple-regge asymptotic discontinuities and will use a generalization of the simple light-cone analysis that we develop in this Section. Consider the box-diagram illustrated in Fig. 4.1.

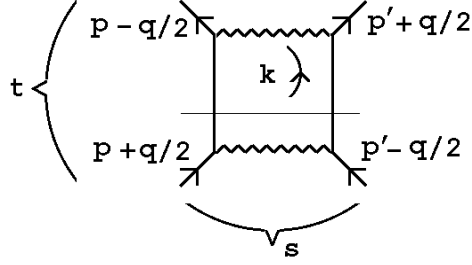


Fig. 4.1 The box diagram.

Initially we ignore the role played by numerators and so we consider, in the notation shown,

$$\begin{aligned}
 I(s, t, m^2) = & \int d^4k [k^2 - m^2 + i\epsilon]^{-1} \left[\left(p - \frac{q}{2} + k \right)^2 - m^2 + i\epsilon \right]^{-1} \\
 & \times [(q - k)^2 - m^2 + i\epsilon]^{-1} \left[\left(p' + \frac{q}{2} - k \right)^2 - m^2 + i\epsilon \right]^{-1}.
 \end{aligned} \tag{4.1}$$

This integral is, of course, a function of invariants only even though it is specified using four momenta. Indeed, we can evaluate the integral using complex, unphysical, momenta that give physical values of the invariants, provided we are careful to define the integral via analytic continuation from the appropriate physical momentum region. Our purpose in this Section is to discuss momentum dependence of this kind for the simplifying case of the leading asymptotic behavior, in a manner that we can apply to much more complicated diagrams in Section 5.

For illustrative purposes we set both $q = 0$ and $m = 0$ in (4.1) and ignore infra-red divergences. We can then write

$$I(s) = \int d^4k [k^2 + i\epsilon]^{-2} [(p + k)^2 + i\epsilon]^{-1} [(p' - k)^2 + i\epsilon]^{-1} \tag{4.2}$$

We choose a particular Lorentz frame and introduce light-cone co-ordinates such that

$$\begin{aligned} p &= \left(\frac{P_+}{2}, \frac{P_+}{2}, 0 \right) + O\left(\frac{1}{s}\right), \quad P_+ \sim s \rightarrow \infty \\ p' &= \left(\frac{P'_+ + P'_-}{2}, \frac{P'_+ - P'_-}{2}, \underline{p}'_{\perp} \right) \end{aligned} \quad (4.3)$$

so that $s = P_+ P'_- [1 + O(1/s)]$. We can then write

$$\begin{aligned} I(s) \underset{s \rightarrow \infty}{\sim} & \frac{1}{2} \int d^2 \underline{k}_{\perp} dk_+ dk_- [k_+ k_- - k_{\perp}^2 + i\epsilon]^{-2} \left[(k_+ + P_+) k_- - \underline{k}_{\perp}^2 + i\epsilon \right]^{-1} \\ & \times \left[(k_+ - P'_+) (k_- - P'_-) - (\underline{k}_{\perp} - \underline{p}'_{\perp})^2 + i\epsilon \right]^{-1} \end{aligned} \quad (4.4)$$

To obtain a non-zero answer by closing the k_+ contour, with k_- and k_{\perp} fixed, the three poles given by the three square brackets of (4.4) must not be on the same side of the contour. This requires $0 < k_- < P'_-$ and, in this case, the k_+ contour can be closed to pick up only the pole in the last bracket. This gives

$$k_+ = P'_+ + \frac{(\underline{k}_{\perp} - \underline{p}'_{\perp})^2 - i\epsilon}{(k_- - P'_-)} \quad (4.5)$$

which is finite and so can be neglected compared to P_+ . Note also that

$$k_- \sim 0, \quad k_{\perp}^2 \sim 0 \quad \Rightarrow \quad k_+ \sim 2k_0 \sim \frac{p'^2}{P'_-} \quad (4.6)$$

(we will need this approximation for the analysis of Section 5). We thus obtain,

$$I(s) \underset{s \rightarrow \infty}{\sim} \pi i \int d^2 \underline{k}_{\perp} [-k_{\perp}^2 + i\epsilon]^{-2} \int_0^{P'_-} dk_- [k_- - P'_-]^{-1} [P_+ k_- - \underline{k}_{\perp}^2 + i\epsilon]^{-1} \quad (4.7)$$

We are specifically interested in the leading real and imaginary parts of (4.7). They are given by the logarithm generated by the pole factor containing P_+ as it approaches the $k_- = 0$ end-point of the integration. If we keep only the integration over $0 < k_- < \lambda P'_-$ and take $\lambda \ll 1$ so that we can make the approximation $k_-/P'_- \sim 0$ we obtain

$$\begin{aligned} I(s) \underset{s \rightarrow \infty}{\sim} & \pi i \int d^2 \underline{k}_{\perp} [-\underline{k}_{\perp}^2 + i\epsilon]^{-2} \frac{1}{P'_-} \int_0^{\lambda P'_-} dk_- (P_+ k_- - \underline{k}_{\perp}^2 + i\epsilon)^{-1} \\ & \sim \frac{1}{P_+ P'_-} [\log(P_+ P'_- \lambda - \underline{k}_{\perp}^2 + i\epsilon) J_1(0)] \\ & \sim \frac{1}{s} [\log(s\lambda + i\epsilon) J_1(0)] \sim \frac{1}{s} [\log s + i\pi] J_1(0) \end{aligned} \quad (4.8)$$

where $J_1(0) \sim \int d^2 \underline{k}_\perp [-\underline{k}_\perp^2 + i\epsilon]^{-2}$ is infinite, but would be finite if we added a mass to the particle propagators.

As we have indicated, the sign of the imaginary part in (4.8) arises directly from the $i\epsilon$ prescription. To obtain the leading imaginary part or, equivalently, the leading behavior of the discontinuity in s , it suffices to keep the $i\epsilon$ dependence while dropping the $-\underline{k}_\perp^2$ dependence in the k_- integral. (4.8) is, of course, independent of λ . It will, however, be useful to note the role of λ with respect to the analytic structure of $I(s)$ in the s -plane. As illustrated in Fig. 4.2, the finite end of the branch-cut associated with the logarithm in (4.8) moves out as $\lambda \rightarrow 0$.

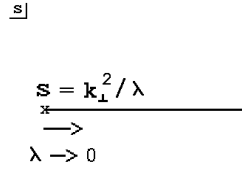


Fig. 4.2 λ -dependence of the branch cut.

This is irrelevant to the asymptotic behavior and the “asymptotic discontinuity” clearly remains unchanged. We will, nevertheless, be able to exploit this simple feature in evaluating multiple discontinuities in the next Section. Also, although (4.8) is an invariant result, for our purposes it will be useful to keep the dependence on both P_+ and P'_- and discuss the dependence of the phase on P_+ .

The initial k_- integration contour for (4.8) is as shown in Fig. 4.3(a) with the pole at $k_- = \underline{k}_\perp^2/P_+$ indicated by a dot.

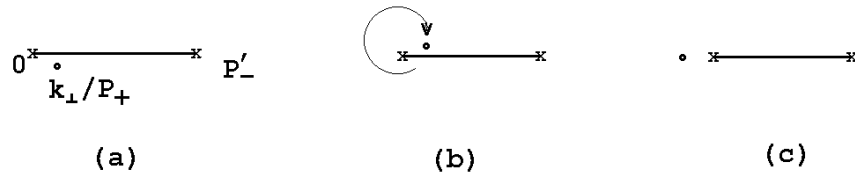


Fig. 4.3 Integration Contours for (a) (4.7) (b) $P_+ \rightarrow e^{2\pi i} P_+$ (c) Fig. 4.4.

As P_+ (and therefore s) completes a circle in the complex plane the pole moves around the end-point as illustrated in Fig. 4.3(b). The result is that the phase of the logarithm in (4.8) changes from π to $-\pi$ and there is a net discontinuity of $2\pi i/s$, as is given directly by (4.8). This is also the result that would be obtained by applying directly the standard cutting rules to Fig. 4.1, cut by the thin line, if the k_+ and k_- integrations are used to put the vertical lines on shell. The above discussion is simply

an asymptotic analysis of how the two cut propagators pinch the integration region to generate a branch-point in s . Introducing λ limits the integration region for the original integral such that the pinching only takes place for $s \sim P_+ > \lambda$. Note also that the residue function $J_1(0)$, multiplying the logarithm in (4.8), is directly obtained from the original box diagram by putting the cut lines giving the discontinuity on-shell using the longitudinal momentum integrations. This is a very simple example (the simplest) of the relationship between a discontinuity and asymptotic behavior.

In evaluating unphysical (multiple) discontinuities in Section 5 we will not assume that the standard cutting rules apply. Instead we will directly analyse the discontinuities produced by logarithms. To understand how a discontinuity generated by a logarithm can provide leading asymptotic behavior we note that the twisted diagram of Fig. 4.4, for $q = 0$, differs from that of Fig. 4.1 only by $P_+ \rightarrow -P_+$.

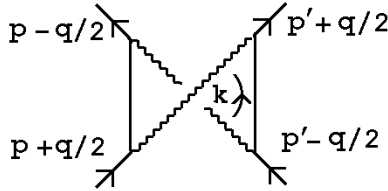


Fig. 4.4 The twisted box diagram.

As a result, the integration contour and pole position of Fig. 4.3(a) is replaced by that of Fig. 4.3(c). In this case a discontinuity is generated for $s < 0$. For $s > 0$ there is no phase generated by Fig. 4.4 and only the real logarithms cancel when this diagram is added to that of Fig. 4.1. The leading behavior of the discontinuity in s , i.e the imaginary part, produced by the diagram of Fig. 4.1 remains. This cancelation of the logarithms is very well-known, of course. It is also well known that the cancelation fails when a non-abelian symmetry group is present and that a consequence is the reggeization of the gluon.

We can briefly summarize the effect of adding numerators to (4.1) as follows. First we note that the numerator of the internal fermion propagator carrying P_+ gives an additional P_+ factor of the form $\gamma_- P_+$. As a consequence, in (4.8), there is the replacement

$$\int_0 dk_- (P_+ k_- + \dots)^{-1} \rightarrow \gamma_- P_+ \int_0 dk_- (P_+ k_- + \dots)^{-1} \sim \log P_+ \quad (4.9)$$

and there is no inverse power of P_+ . Also, each coupling to a gluon gives a γ matrix factor and since the external fermion lines are on-shell we can use the asymptotic

form of the Dirac equation (i.e. $\gamma_- P_+ \psi \sim m \psi$) to write

$$\begin{aligned}
\langle P_+ | \gamma_\mu \gamma_- \gamma_\nu | P_+ \rangle &\sim \langle P_+ | \frac{\gamma_- P_+}{m} \gamma_\mu \gamma_- \gamma_\nu \frac{\gamma_- P_+}{m} | P_+ \rangle \\
&= \langle P_+ | P_+ \gamma_- P_+ | P_+ \rangle / m^2 \sim P_+ / m
\end{aligned} \tag{4.10}$$

This gives another power of P_+ ($\sim s$) provided that the corresponding factor of P'_- is present in the finite momentum part of the scattering process. Not surprisingly this factor emerges from that part which would dominate if P'_- were large. However, we want to emphasize that this selection is made only by the need to form a Lorentz invariant amplitude from the non-invariant large momentum process.

Finally we note that the above analysis goes through with very little modification if we take both m^2 and q to be non-zero so that (4.2) will not be infra-red divergent.

5. UNPHYSICAL TRIPLE DISCONTINUITIES AND HIGHER-ORDER GRAPHS

In this Section we generalize the analysis of the last Section to asymptotic triple discontinuities. The essential idea is that there is a well-defined leading-log result for each triple discontinuity, just as there was for the single discontinuity in s in the last Section, and that this can be found from the leading-log calculation of an amplitude by keeping the $i\epsilon$ dependence of all logarithms.

We begin by considering again the maximally non-planar graph shown in Fig. 3.1. To understand how asymptotic discontinuities of the kind we are interested in arise, we first consider a physical region discontinuity. To this end we interchange P_1 and $P_{1'}$ in (3.1) so that $P_{1'}$ and P_2 are the momenta of incoming particles. For simplicity, we also set $Q_i = 0$, $i = 1, 2, 3$. This could cause confusion as to which invariants discontinuities actually occur in. However, for the discontinuities that interest us, we will be able to avoid this issue. (As in the previous Section, adding both transverse momenta and masses to our discussion would not change the essential features of the analysis, but would eliminate gluon infra-red divergences. We will discuss, at some points, the general effect of adding transverse momenta.) Therefore we write, asymptotically,

$$\begin{aligned}
 P_{1'} &\rightarrow -P_1 = (p_{1'}, p_{1'}, 0, 0) , & p_{1'} &\rightarrow \infty \\
 P_2 &\rightarrow -P_{2'} = (p_2, 0, p_2, 0) , & p_2 &\rightarrow \infty \\
 P_3 &\rightarrow -P_{3'} = (p_3, 0, 0, p_3) , & p_3 &\rightarrow \infty
 \end{aligned}
 \tag{5.1}$$

Since we will ultimately be looking for a symmetric triple discontinuity, we consider only routes for the internal loop momenta of Fig. 3.1 that are completely symmetric with respect to the three external loops. There is essentially only one possibility. The two apparently distinct possibilities illustrated in Fig. 5.1 are related by interchanging the primed and unprimed external momenta. We will also want to make a symmetric choice for the quark lines we place on shell. Although we will not discuss the anomaly in detail until the next Section, we note that a product of three orthogonal γ -matrices must be associated with the process of putting on-shell each internal quark line. To achieve this it is necessary to put on-shell, symmetrically, the internal lines in Fig. 5.1(a) along which a single loop momentum flows. Therefore, we consider only such lines in the following.

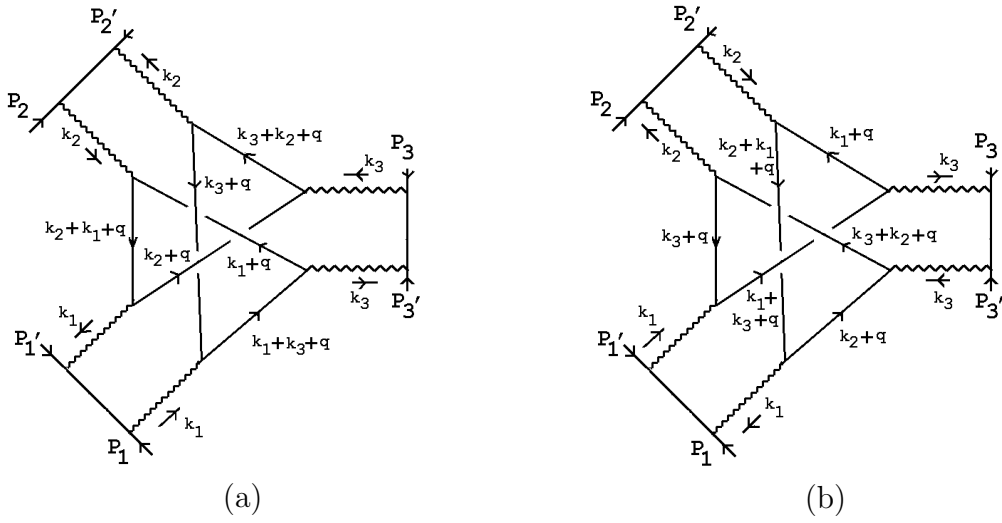


Fig. 5.1 Routing Loop Momenta for Fig. 3.2.

Using the momentum routing of Fig. 5.1(a) and the analysis of the previous Section we consider logarithms generated by the k_1 and k_2 integrations. The k_1 and k_2 loops are shown in Fig. 5.2.

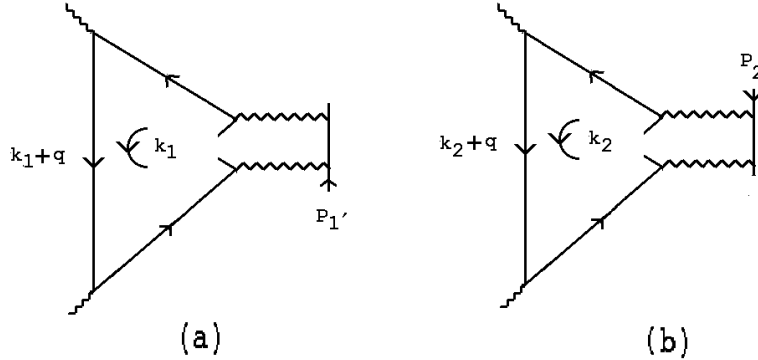


Fig. 5.2 (a) The k_1 Loop (b) The k_2 Loop.

For the moment, we omit the propagators in the sloping lines and all propagator numerators. (The omitted propagators will, nevertheless, play an important role below. They are also relevant if we wish to consider the other kinds of discontinuities that appear in Fig. 3.3.) In this case, the two loops differ only in the light-cone direction of P_1' and P_2 .

We consider Fig. 5.2(a) first. We can directly apply the discussion following (4.4) if we identify P_1' with p , q with p' , k_1 with k , and consider the propagator pole

at $(k_1 + q)^2 = 0$. We then obtain

$$\begin{aligned} I(p_1' q_{1-}) &\sim i \int d^2 \underline{k}_{1\perp} [-k_{1\perp}^2 + i\epsilon]^{-2} \int_0^{\lambda q_{1-}} dk_{1-} [k_{1-} - q_{1-}]^{-1} [p_1' k_{1-} - \underline{k}_{1\perp}^2 + i\epsilon]^{-1} \\ &\sim \frac{1}{p_1' q_{1-}} \log [p_1' \lambda q_{1-} + i\epsilon] \end{aligned} \quad (5.2)$$

We have used the notation (used extensively in the following) that for any four-momentum k

$$k_{i-} = k_0 - k_i \quad \underline{k}_{i\perp} = (k_j, k_k) \quad j \neq k \neq i \quad i, j, k = 1, 2, 3 \quad (5.3)$$

The q_{1-} dependence indicates that the logarithm is a reflection of a threshold in the invariant $P_{1'} \cdot q$. This dependence plays an important role in the following discussion. We also retain the λ -dependence, for technical reasons that will become apparent later. The final result will be independent of λ , as it must be. From Fig. 5.2(b) we analogously obtain

$$I(p_2 q_{2-}) \sim \frac{1}{p_2 q_{2-}} \log [-p_2 \lambda q_{2-} + i\epsilon] \quad (5.4)$$

The minus sign appears relative to (5.2) because of the opposite direction of P_2 .

Next we consider how the logarithmic branch cuts generated by the k_1 and k_2 integrations can trap the internal loop integration over q to produce an overall discontinuity in $s_{1'2} \sim p_1' p_2$. For simplicity, we consider the region where

$$\underline{k}_{i\perp}^2 \sim q^2 \sim 0 \quad i = 1, 2, 3 \quad (5.5)$$

Appealing to (4.6) we can then, for our present purposes, effectively ignore the remaining k_i dependence of the quark loop (including the propagators that we ignored in the above discussion). If we parameterize q as

$$q = \left(q_0, q_{1-}, q_{2-}, q_{3-} \right) \quad (5.6)$$

we can treat the q_{i-} as independent variables, with q_0 essentially determined by the constraint $q^2 \sim 0$. The logarithmic cuts of (5.2) and (5.4) appear, respectively, in the q_{1-} and q_{2-} planes and if we make a further change of variables to

$$q_{1-} = x_2 x_3, \quad q_{2-} = x_3 x_1, \quad q_{3-} = x_1 x_2 \quad (5.7)$$

the two branch points appear in the x_3 -plane, for fixed, positive, x_1, x_2 , as illustrated in Fig. 5.3(a).

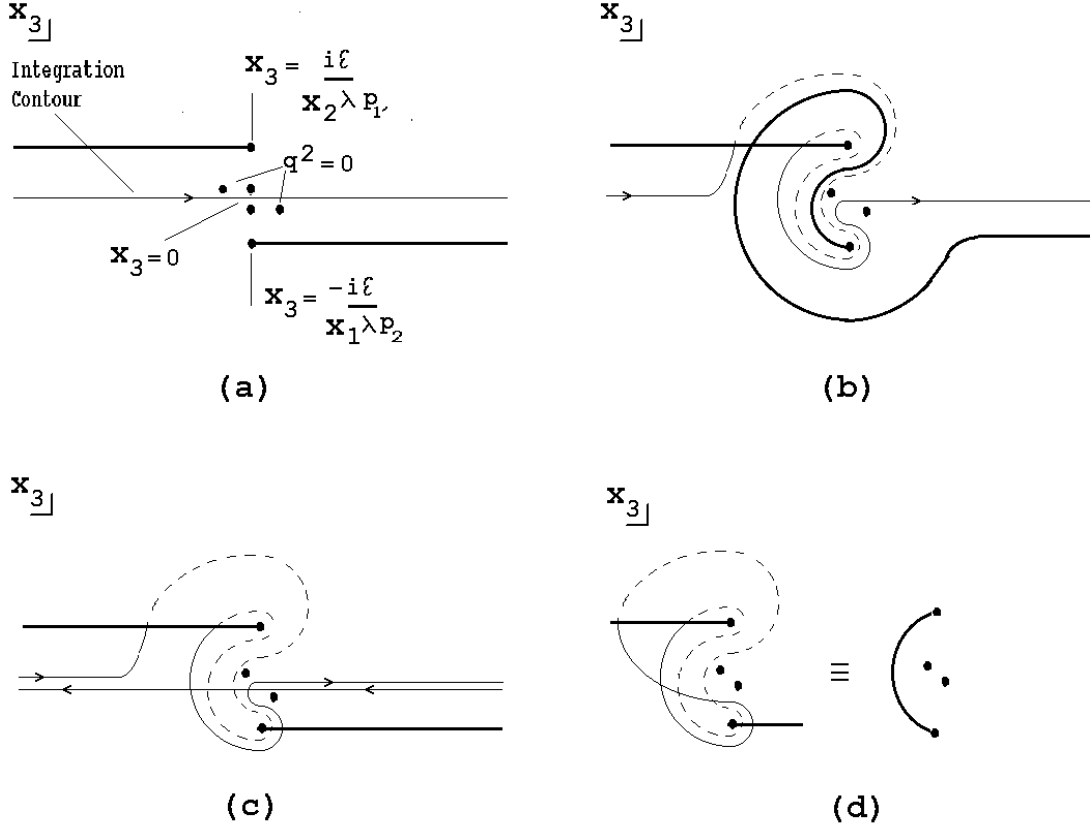


Fig. 5.3 Contours in the x_3 -plane (a) the initial contour (b) $p_2 \rightarrow e^{2\pi i} p_2$ (c) the discontinuity (d) the discontinuity as a line integral.

(The branch points also appear, separately, in the x_2 and x_1 planes. To focus on the $s_{1/2}$ discontinuity and avoid any complication from discontinuities involving a logarithm of p_3 in these planes we can take the λ for this logarithm to be much smaller.) The propagator poles that are not on-shell, that we ignored in the above discussion, combine to give a multiple pole at $q^2 = 0$ (on both sides of the contour, as determined by the presence of $i\epsilon$ in all propagators). If we continue to ignore propagator numerators then the factors of $1/q_{1-}$ and $1/q_{2-}$, in (5.2) and (5.4) respectively, will also contribute poles at $x_3 = 0$ (that will partly be compensated by the jacobian due to the change of variables). However, in the anomaly contribution we will ultimately consider, these poles will be directly canceled by numerator factors.

The threshold we are interested in occurs when the two branch points collide (at $x_3 = 0$ for $\epsilon = 0$). To extract the discontinuity we consider a full-plane rotation of p_2 , with $p_{1'}$ fixed, so that the logarithmic branch-cut (5.4) deforms the contour as shown in Fig. 5.3(b) - the dashed line indicates that the contour is on the second sheet of the branch-point (5.2). (We have omitted the poles at $x_3 = 0$.) Note that the continuation path we have chosen isolates the discontinuity around the $s_{1/2}$ branch

cut, since it avoids the pinching of the integration contour with the singularity at $q^2 = 0$ that would give other discontinuities. The desired discontinuity is obtained by adding the original contour in the opposite direction, as shown in Fig. 5.3(c). Combining both contours we obtain Fig. 5.3(d) which, as illustrated can be written as a line integral between the two branch points of the double-discontinuity due to both cuts. As $\epsilon \rightarrow 0$, or in the asymptotic limit $p_{1'}, p_2 \rightarrow \infty$, the branch points approach each other and the result is a closed contour integral around the singularity at $q^2 = 0$ which is independent of the position of the end points and remains finite in the asymptotic limit. This is the asymptotic discontinuity and the singularity at $q^2 = 0$ is clearly crucial in producing a non-zero result.

In Fig. 5.4(a) we have illustrated the effect of adding (external and internal) transverse momenta in the the foregoing analysis. The integral between the branch points, of the double discontinuity, is still obtained, while the singularity at $q^2 = 0$ separates into a set of poles at both positive and negative x_3 .

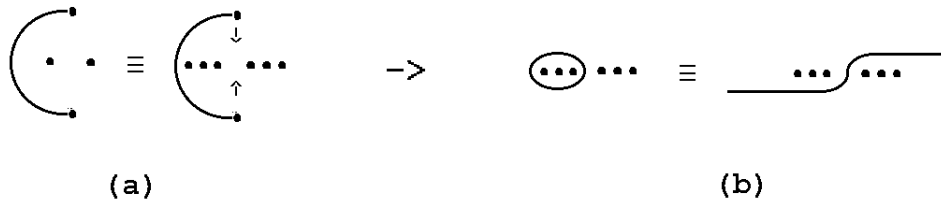


Fig. 5.4 (a) The x_3 contour with finite transverse momenta (b) equivalence of the asymptotic contour to the original contour.

In Fig. 5.4(b) we have shown the asymptotic discontinuity. Since the branch points are logarithmic, the double discontinuity involved is simply $4\pi^2$ and so no longer contains either branch cut. Consequently, the asymptotically finite integral around the poles to the left can be opened up to give the original contour, as illustrated. (If there is a singularity at $x_3 = 0$, the contour is constrained to pass through this point although, as we noted above, for the anomaly contribution to graphs, this will not be the case). The final result shown in Fig. 5.4(b) is just what would be given by the normal cutting rules for a discontinuity in $s_{1'2}$, i.e. the original integral with the four propagators involved in generating the discontinuity placed on-shell. Note that the same result is obtained if the discontinuity is evaluated by varying $p_{1'}$. An integral around the positive x_3 poles appears at the intermediate stage, which can then be opened up to give the same final contour as in Fig. 5.4(b).

An obvious, but essential, requirement in the origin of the asymptotic discontinuity, which we want to emphasize, is that the branch-cuts due to the logarithms in $p_{1'}$ and p_2 must lie on opposite sides of the x_3 contour. In a physical region this requirement is normally straightforward for a loop integration producing a threshold

due to two massive states since the loop momentum will flow oppositely through the two states and the $i\epsilon$ prescription will place the states on opposite sides of the energy integration contour. In the variables we are using the generation of the threshold is a little more subtle. Note, for example, that when $x_1 < 0$ the branch-point (5.2) appears in the upper half-plane (moving through infinity as x_1 moves through zero) and there is no discontinuity. Therefore, the signs of the x_i play an essential role in the occurrence of the discontinuity. A further requirement, which clearly holds in the case just discussed, is that the trapping (pinching) of the contour that we have discussed must combine with the pinching associated with the logarithms to give a complete cut through the diagram. That is to say, the complete set of pinchings must correspond to an overall invariant cut.

We consider next the unphysical discontinuities that are our principal interest. According to the discussion in Section 3, we are looking for a triple discontinuity of the form of Fig. 3.4 that treats the three cut lines of the quark loop symmetrically so that, in a physical region, the sign of the energy component can be the same for all three on-shell states. We will, therefore, confine our discussion to a search for a symmetric triple discontinuity. As we noted, if the normal cutting rules apply there is no triple discontinuity (symmetric or not) of the Fig. 3.4 kind. We consider whether the direct evaluation of discontinuities gives the same result.

The discontinuity we discussed above occurred in a physical region that is unsymmetric in that P_2 is the momentum of an incoming particle while P_1 is the momentum of an outgoing particle. To look for a symmetric discontinuity we will use an analysis that treats the complete graph symmetrically throughout. To this end, we will start in the symmetric asymptotic region (3.1) where all momenta are real and

$$s_{ij} \sim -p_i p_j < 0 \quad (5.8)$$

In this region, the diagram is defined by the usual $i\epsilon$ prescription. Since all three invariants must be positive, the triple discontinuity of Fig. 3.4 can only be present in the triple-regge limit if we allow the large momenta involved to be unphysical. A symmetric way to do this is to start from the real physical region and take

$$p_i \rightarrow e^{-i\pi/2} p_i = ip_i, \quad i = 1, 2, 3 \quad \Rightarrow s_{ij} \sim (-ip_i)(ip_j) > 0 \quad (5.9)$$

Given the symmetry of the present discussion, it is immediately apparent that there will not be a (symmetric) triple discontinuity, as we now show. Using the above analysis, logarithms will be generated by each of the k_i integrations. If we consider again the region where the transverse momenta are close to zero then, from (4.6), the requirement that the energy component of each on-shell line in the loop have the same sign is equivalent to requiring that the q_i^- all have the same sign. This, in turn, requires that the x_i should all have the same sign. However, in the symmetric real

physical region, if x_1 and x_2 have the same sign, the logarithmic branch cuts in P_1 and P_2 lie on the same side of the x_3 contour as illustrated in Fig. 5.5.

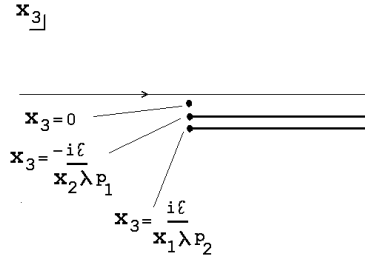


Fig. 5.5 The Symmetric Location of Branch-Cuts in the x_3 -plane.

Since the continuation (5.9) is symmetric they will remain on the same side after the continuation. As a consequence, in the symmetric x_i region, the contour will not be trapped and distorted as one branch point moves around the other, as it was in Fig. 5.3, and no discontinuity will result. We conclude therefore that, for the graph we are discussing, discontinuities can only be generated in asymmetric regions of the x_i that can not provide the symmetric triple discontinuity that we are looking for.

The foregoing analysis also precludes the occurrence of a triple discontinuity, that is appropriately symmetric, in the diagram of Fig. 3.5. To obtain a symmetric triple discontinuity we look for a graph that has the appropriate overall symmetry and also, for each $i \neq j \neq k$, has logarithmic branch cuts on both sides of the x_i contour in a symmetric region of x_j and x_k . With these requirements in mind, an obvious graph to consider is that of Fig. 3.7. To discuss this graph we continue, for simplicity, to take $Q_1 = Q_2 = Q_3 = 0$. Two symmetric (distinct) routes for the internal momenta are shown in Fig. 5.6. For a threshold corresponding to the cutting of particular lines of the internal quark loop to be generated the external loop momentum generating the relevant logarithms must pass through at least one of the lines. With this constraint, only the routing shown in Fig. 5.6(a) will give both discontinuities of the kind we are looking for and the γ -matrix structure for on-shell contributions that we show, in the next Section, gives the anomaly. The routing of Fig. 5.6(b) would be appropriate for discussing the triple discontinuity of Fig. 3.6. However, in this case the γ -matrix structure needed to generate the anomaly does not appear in the on-shell contributions. Therefore, the triple discontinuity of Fig. 3.6 does not contain the anomaly.

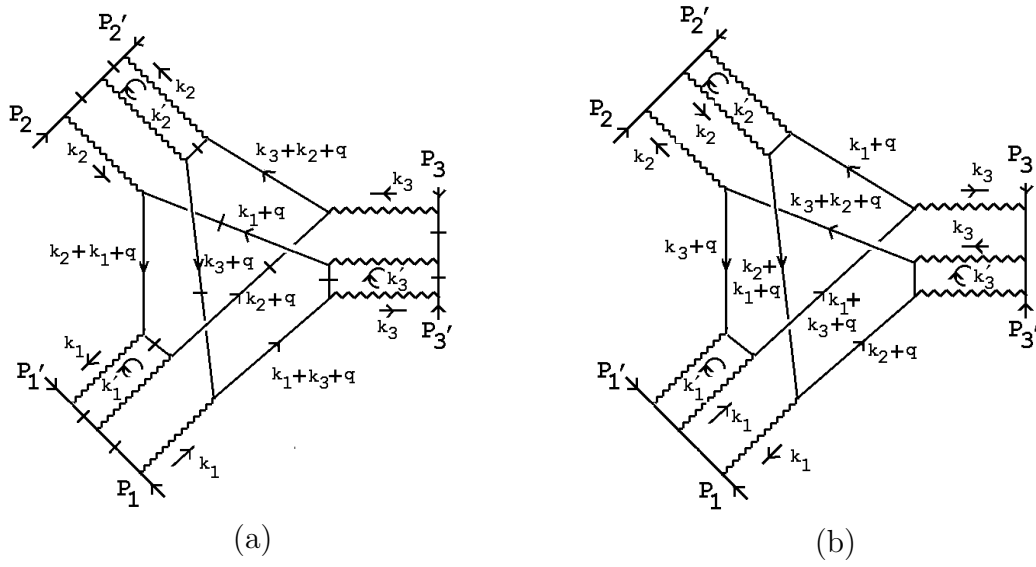


Fig. 5.6 Labeling Momenta for Fig. 3.7.

Using the momentum routing of Fig. 5.6(a) we consider the logarithms generated by both the k_i and k'_i loop integrations. Extracting all logarithms places on-shell all the hatched lines of Fig. 5.6(a), and gives leading behavior of the form of (3.2) multiplied by double logarithms of each of the P_{i+} . At the diagrammatic level (i.e. temporarily discussing diagrams rather than discontinuities), we anticipate that existing calculations can be adapted to show that the double logs are canceled by adding diagrams of the kind illustrated in Fig. 5.7. That is, we add diagrams containing twists relative to Fig. 3.7, as in Figs. 5.7(a) and (b) together with diagrams, such as that in Fig. 5.7(c), that produce the well-known cancelations necessary for reggeization.

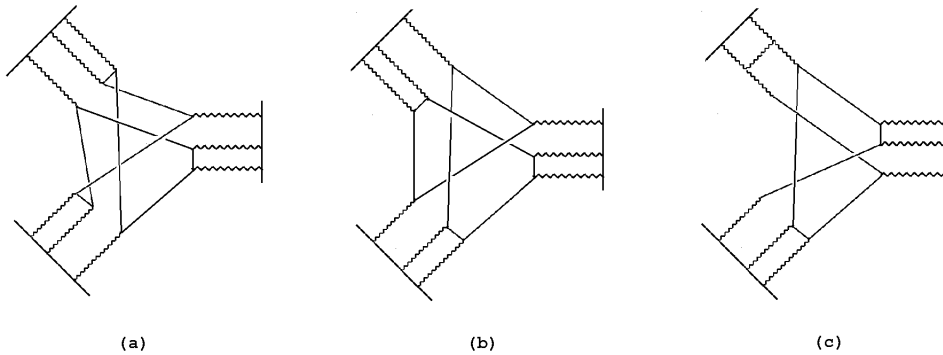


Fig. 5.7 Diagrams with (a) Twisted k'_i Loops (b) Twisted k_i Loops (c) Reggeization Cancelations

After the double logs are canceled, the remaining single logs should go into reggeization contributions, in analogy with Fig. 3.6, with the remaining terms providing new lowest-order reggeon interactions. As we have emphasized repeatedly, to discuss this systematically we consider multiple asymptotic discontinuities rather than the behavior of full diagrams. We do this, as above, by keeping the q -dependence of all logarithms together with all $i\epsilon$ dependence. We consider specifically the logarithms generated by the k_1 and k'_1 loops, but the symmetry of the diagram obviously determines that the others can be treated identically. The loops, extracted from Fig. 5.6, are shown in Fig. 5.8. The k_1 loop is identical to those of Fig.5.2 and can be evaluated analogously.

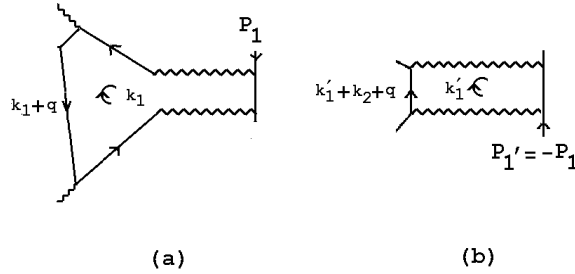


Fig. 5.8 (a) The k_1 Loop (b) The k'_1 Loop.

Using a similar analysis, the k'_1 loop gives an integral of the form

$$\int_0^{(k_2+q)_1-} dk'_{11-} \dots \quad (5.10)$$

If we again go to the region where all transverse momenta are close to zero then, using (4.6), it follows that after the k_2 integration

$$k_{21-} \sim k_{20} \sim q^2/q_{2-} \ll q_{1-} \quad (5.11)$$

Therefore, we can take the upper end-point in (5.10) to be q_{1-} . In this case both the k_1 and k'_1 integrations give logarithms with q_{1-} in the argument - but with opposite signs. We then have branch-cuts located as in Fig. 5.9(a) in each of the x_1, x_2 and x_3 planes. We have included poles at $q^2 = 0$ and $x_i = 0$ and have used different λ_i and λ'_i for each branch-cut to allow us to separate the branch points in our discussion.

With values of the λ_i and λ'_i implied by Fig. 5.9(a), we could clearly obtain a discontinuity in $s_{jk'}$ (due to the two closest branch points) by repeating the discussion illustrated by Fig. 5.3. The discontinuity would similarly be an integral between the two branch points involved, as in Fig. 5.3(d), but because of the additional branch points that are present, the contour could not be opened up as in Fig. 5.4. Therefore, having taken $x_j, x_k > 0$ so that the branch cuts lie as in Fig. 5.9(a), the discontinuity would involve only pure imaginary or negative real part values of x_i .

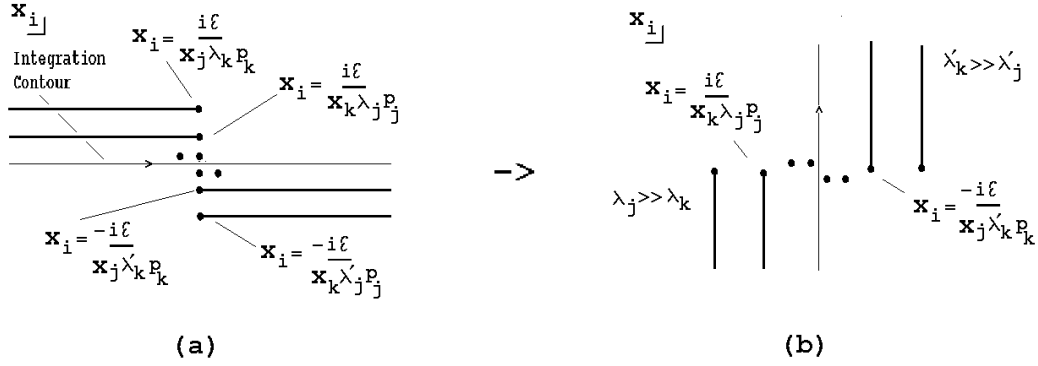


Fig. 5.9 (a) Branch Points in the x_i -plane (b) $p_i \rightarrow e^{-i\pi/2} p_i = ip_i$, $i = 1, 2, 3$

Consequently, any further discontinuity obtained by the collision of branch points in the x_j or x_k planes would have to involve mixed real part signs for the x_i . We conclude (not surprisingly) that in the physical region a triple discontinuity can not be obtained that involves only positive values of all three x_i .

This brings us to the central point of the paper. If we go to the unphysical region (5.9), where we expect to encounter an unphysical triple discontinuity, the last analysis changes in a crucial manner. The resulting location of branch cuts is now as shown in Fig. 5.9(b), allowing the integration contour to be rotated as illustrated. In Fig. 5.9(b) we have also, for emphasis, chosen significantly different values of the λ_i and λ'_i . If we again determine the discontinuity associated with the collision of the two nearest branch points, as above, the result will be the contour integral of the double discontinuity shown in Fig. 5.10.

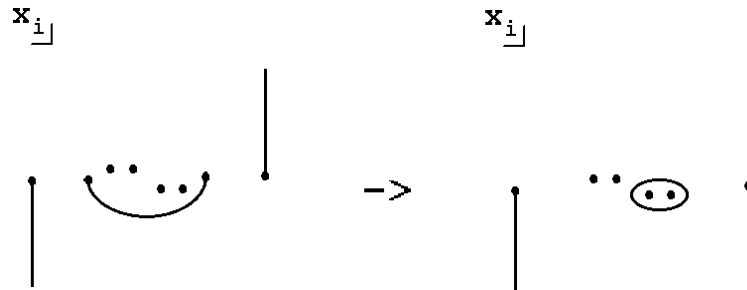


Fig. 5.10 The unphysical region discontinuity.

Now the integral involves positive real values of x_i and, as illustrated, the asymptotic limit gives a loop integral over just positive values. The contour integral can not be opened up, however, since the other branch cuts remain.

Having derived a first discontinuity from two branch points in the x_i plane, as in Fig. 5.10, it is straightforward to keep the remaining branch points and move on to the x_j and x_k planes where, in each case, only two branch cuts now appear. In both

planes, discontinuities of the form of Fig. 5.10 occur, provided the x_i integration is restricted to positive real values. Therefore, we obtain a triple discontinuity in which each of the x_i , x_j and x_k integrations is consistently over positive values and the asymptotic contour is obtained as illustrated by the first two contours in Fig. 5.11.



Fig. 5.11 Contours for the x_i , x_j and x_k integrations.

Since all logarithmic branch cuts are now removed, all three contours can be opened up to obtain the last contour of Fig. 5.11 which is, once again the original contour of integration for each of x_i , x_j and x_k . We thus obtain a triple discontinuity which, at first sight, corresponds to the usual cutting rules since all cut lines are on-shell. However, there is a subtlety.

If we consider the discontinuity arising from the pinching of logarithms of $p_1\lambda_1$ and $p_2\lambda'_2$, for example, then the lines put on-shell in the discontinuity are those that have thick hatches in Fig. 5.12(a).

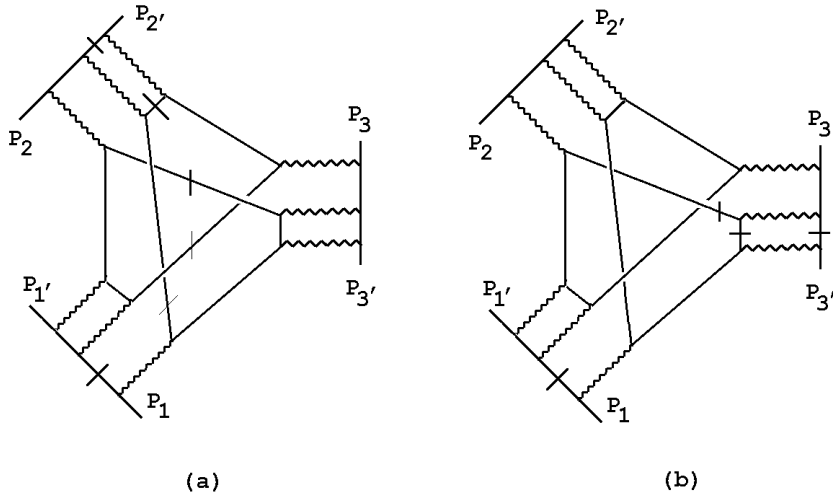


Fig. 5.12 On-shell lines for (a) an $s_{12'}$ discontinuity (b) a potential $s_{13'}$ discontinuity.

These lines are only a subset of those required to obtain a complete cut of the diagram. This implies that the corresponding pinching does not, by itself, give a singularity of the complete integral and a-priori the integration contour could be deformed away

from the pinched region. To obtain a complete cut we must add the lines that have thin hatches in Fig. 5.12(a). When these lines are on shell the pinching does give an overall singularity. But, if we require a common sign for the x_i the two thin-hatched lines actually have the wrong $i\epsilon$ prescription to straightforwardly combine with the asymptotic pinching to give what would be a physical sheet “asymptotic normal threshold”. However, each of the two thin hatched lines is separately placed on shell by one of the additional discontinuities. Therefore, a triple discontinuity of the kind we have found does correspond to the triplet $\{s_{12'}, s_{23'}, s_{32'}\}$ of invariant cuts.

Note that if we consider instead the discontinuity arising from the pinching of logarithms of $p_1\lambda_1$ and $p_3\lambda_3'$ then the lines put on shell are those hatched in Fig. 5.12(b). In this case there is no simple way to include additional lines and obtain an invariant cut. Therefore, this pinching can not be extended to a complete cut of the diagram. We conclude that the triple discontinuity in $\{s_{12'}, s_{23'}, s_{32'}\}$ that is illustrated in Fig. 3.7 is the only combination that exists, as an extension of the above analysis. It is symmetric, with each of the internal quark lines that are put on shell by k_i integrations treated symmetrically. All three of these lines contribute to each invariant cut but, as we have just discussed, two of them always have the wrong $i\epsilon$ prescription, relative to the third, to give a physical normal threshold. Singularities associated with combinations of forward and backward going particles (as the mixture of $i\epsilon$ prescriptions implies is the case) are “mixed- α ” solutions of the Landau equations[10] and are referred to as pseudothresholds. In general, pseudothresholds are not singular on the physical sheet, just because of the conflicting $i\epsilon$ prescriptions. However, they are generally singular on unphysical sheets and can appear in multiple discontinuities. For the unphysical multiple discontinuity we are discussing, a combination of “asymptotic pseudothresholds” can contribute when the same combination of normal thresholds can not.

6. THE TRIANGLE ANOMALY

In this Section we give a brief discussion of how the anomaly occurs in the triple discontinuity of Fig. 3.7. A complete discussion would be obtained by a straightforward generalization, to include the minor additional complexities, of the lengthy analysis of Fig. 3.1 in [3].

All the cut lines of Fig. 3.7 are on-shell, as described in the last Section. We begin by adding in the numerator dependence that we essentially ignored in the previous Section. For the external lines, additional powers of the external momenta are generated as in (4.9) and (4.10). As a result, inverse external momentum factors, such as $p_1'^{-1}$ in (5.2) and p_2^{-1} in (5.4) are eliminated and the factor of $P_1+P_2+P_3+$ that appears in (3.2) is produced. Also, if we use the natural transverse momenta given by (5.3), the light-like γ -matrix couplings that appear at each of the vertices of the internal loop (after the triple-regge limit is taken) are as illustrated in Fig. 6.1(a). For the hatched lines that appear in both Fig. 6.1(a) and (b), we keep the γ matrices shown. These are the “local couplings” (see [3]) that appear when that part of the associated numerator is kept that cancels the internal momentum factors, such as q_1^{-1} in (5.2) and q_2^{-1} in (5.4), that arise from the longitudinal loop momentum integrations.

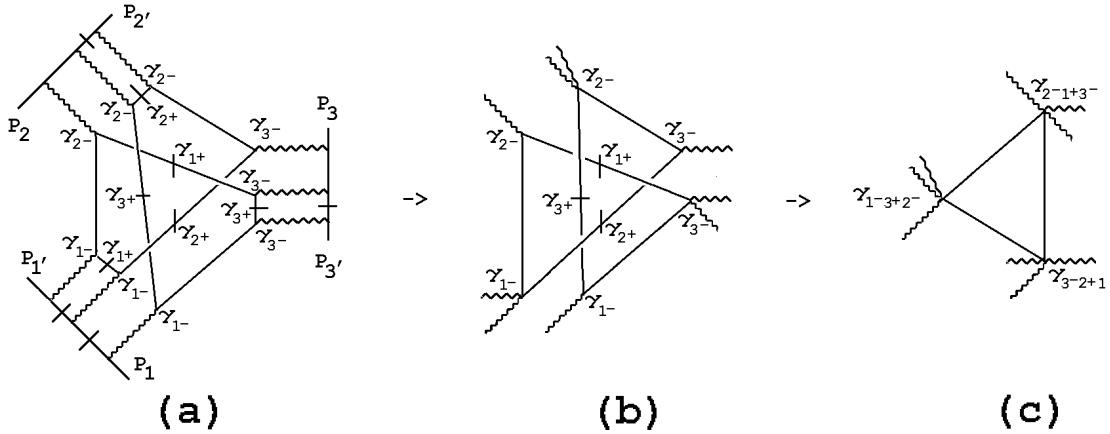


Fig. 6.1 γ -matrix structure for the reggeon interaction extracted from Fig. 3.7.

The resulting asymptotic behavior then has the form

$$\begin{aligned}
P_{1+} P_{2+} P_{3+} & \prod_{i=1}^3 \int \frac{d^2 k_{i1} d^2 k_{i2} d^2 k_{i3}}{k_{i1}^2 k_{i2}^2 k_{i3}^2} \delta^2(Q_{i\perp} - k_{i1} - k_{i2} - k_{i3}) G_i^3(k_{i1}, k_{i2}, k_{i3} \cdots) \\
& \times R^9(Q_1, Q_2, Q_3, k_{11}, k_{12}, k_{13} \cdots)
\end{aligned} \tag{6.1}$$

where R^9 is the triangle diagram illustrated in Fig. 6.1(c).

By comparing with the three-reggeon version of (3.6) and (3.7) we can extract R^9 as a nine-reggeon interaction which, if we now write

$$k_{i1} = q_i + k_i, \quad k_{i2} = q_i - k_i - k'_i, \quad k_{i3} = k'_i, \tag{6.2}$$

can be written (very similarly to (3.4)) as

$$\begin{aligned}
R^9(q_1, q_2, q_3, k_1, k_2, k_3, k'_1, k'_2, k'_3) = \\
\int d^4 k \frac{\text{Tr}\{\gamma_5 \gamma^{1^- 3^+ 2^-} (\not{k} + \not{k}_1 + \not{q}_2 + \not{k}_3) \gamma_5 \gamma^{2^- 1^+ 3^-} \not{k} \gamma_5 \gamma^{3^- 2^+ 1^-} (\not{k} - \not{k}_2 + \not{q}_1 + \not{k}_3)\}}{(k + k_1 + q_2 + k_3)^2 k^2 (k - k_2 + q_1 + k_3)^2}
\end{aligned} \tag{6.3}$$

where

$$\begin{aligned}
\gamma^{1^- 3^+ 2^-} &= \gamma_{1^-} \gamma_{3^+} \gamma_{2^-} = \gamma^{-, -, -} - i \gamma^{-, -, +} \gamma_5 \\
\gamma^{2^- 1^+ 3^-} &= \gamma_{2^-} \gamma_{1^+} \gamma_{3^-} = \gamma^{-, -, -} - i \gamma^{+, -, -} \gamma_5 \\
\gamma^{3^- 2^+ 1^-} &= \gamma_{3^-} \gamma_{2^+} \gamma_{1^-} = \gamma^{-, -, -} - i \gamma^{-, +, -} \gamma_5
\end{aligned} \tag{6.4}$$

and $\gamma^{\pm, \pm, \pm}$ is defined by (3.5).

Because of the symmetric choice of co-ordinates and the completely symmetric manner in which we have evaluated the triple discontinuity, the anomaly appears in a slightly different way to that discussed for Fig. 3.1 in [3]. To obtain the anomaly divergence we must have a component of the axial-vector triangle diagram tensor $\Gamma^{\mu\nu\lambda}$ with $\mu = \nu$ having a lightlike projection and λ having an orthogonal spacelike projection. There must also be a transverse momentum (scaled to zero) in the remaining orthogonal spacelike direction. If we choose the γ_5 component from all three vertices, the first requirement is not met. However, if we choose the γ_5 component from one of the three vertices in Fig. 6.1(c), and choose the vector coupling from the other two vertices, it is met. The finite light-like momentum involved must then have a projection on $n^{-, -, -\mu}$ and the orthogonal spacelike momentum must be distinct in each case. The three distinct possibilities for the anomaly to occur are associated with the three distinct hexagraphs described in [3], and hence with three distinct helicity amplitudes. We will discuss this relationship further in our later papers.

As we discussed at length in [3], while the triple discontinuity giving the interaction of Fig. 6.1 occurs in an unphysical region, the interaction will, nevertheless, provide a “real” reggeon interaction in physical regions. Because the discontinuity has the symmetry property that we emphasized in previous Sections, the anomaly infra-red divergence can occur in the physical-region configuration shown in Fig. 6.2. (The large dots indicate that a local interaction is involved.) The γ_5 interaction is at the intermediate vertex and the light-like momenta are as in(3.10)-(3.14). Fig. 6.2 can then be identified with the basic anomaly process of Fig. 3.2 except that, as anticipated in Section 3, there is an additional wee gluon involved. There are also additional gluons with finite transverse momentum.

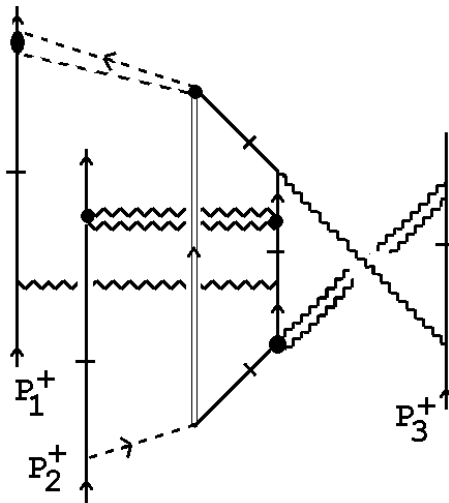


Fig. 6.2 Physical region configuration for the anomaly divergence in Fig. 6.1.

If there are no reggeization logarithms of the same order that appear accompanying the anomaly, as our discussion in Sections 3 and 5 implies, then that part of the triple discontinuity interaction given by Fig. 6.1 that contains the anomaly will appear as the leading triple-regge coupling of the three three-reggeon states. All other diagrams that contribute will then have a similar triple discontinuity. The discussion in Section 5 shows that such diagrams must have “right-hand and left-hand” cuts in each x_i -plane, suggesting that only diagrams having the same structure as that of Fig. 3.7, but with incoming and outgoing lines switched, can contribute. If this is the case, signature conservation will occur, requiring an additional reggeon in at least one channel. In this paper we will not introduce color factors, except to note that we expect every reggeon state coupling to the anomaly to carry anomalous color parity. This will ensure that the anomaly does not occur in the scattering of elementary quarks and gluons - as we have anticipated. Instead the scattering states must have an essential “non-perturbative” wee-parton content that ensures they can scatter by exchanging reggeon states coupling to the anomaly.

We will postpone all further discussion of cancelations to our following papers. The purpose of this paper has been to establish that a class of diagrams contain a multiple discontinuity that does generate the reggeon interaction anomaly. For the moment we note only that when the $SU(3)$ gauge symmetry of QCD is broken to $SU(2)$ the infra-red divergence that involves the anomaly and that actually dominates bound-state interactions occurs in diagrams that are very similar to the ones we have discussed. An example, corresponding to a triple-regge multi-pomeron interaction, is shown in Fig. 6.3.

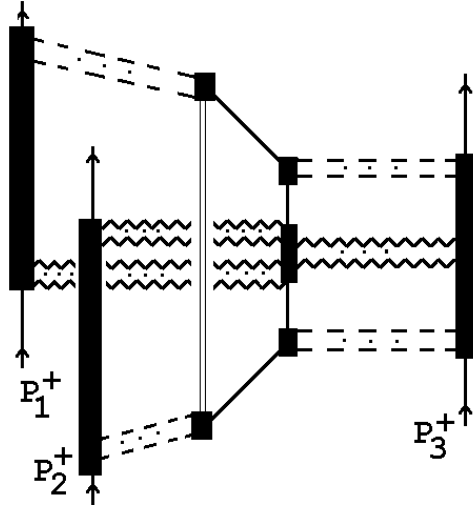


Fig. 6.3 The anomaly configuration in bound state interactions.

The scattering states are bound-states and the solid, wavy, lines are, reggeized, massive gluon states that are $SU(2)$ singlets. The dashed lines represent massless gluons carrying zero transverse momentum. In this situation the three multi-reggeon (pomeron) states that are interacting through the anomaly all have a wee-parton component that participates in the divergence.

References

- [1] M. F. Atiyah, in *Anomalies, Geometry and Topology*, edited by W. A. Bardeen and A. R. White (World Scientific, Singapore, 1985); R. Jackiw, *ibid.* and in *Effects of Dirac's Negative Energy Sea Quantum Numbers*, Dirac Prize lecture, March 1999, hep-th/9903255.
- [2] G. 't Hooft, *Phys. Rep.* **142**, 357 (1986).
- [3] A. R. White, *Phys. Rev.* **D63** 016007, (2001), **D58**, 074008 (1998).
- [4] A. R. White, *Nucl. Phys. Proc. Suppl.* **96**, 277-286 (2001) - hep-ph/0008267; see also Lectures in the Proceedings of the Theory Institute on Deep-Inelastic Diffraction, Argonne National Laboratory (1998).
- [5] E. A. Kuraev, L. N. Lipatov, V. S. Fadin, *Sov. Phys. JETP* **45**, 199 (1977); J. B. Bronzan and R. L. Sugar, *Phys. Rev.* **D17**, 585 (1978), this paper organizes into reggeon diagrams the results from H. Cheng and C. Y. Lo, *Phys. Rev.* **D13**, 1131 (1976), **D15**, 2959 (1977); V. S. Fadin and V. E. Sherman, *Sov. Phys. JETP* **45**, 861 (1978); V. S. Fadin and L. N. Lipatov, *Nucl. Phys.* **B477**, 767 (1996) and further references therein; A. R. White, *Int. J. Mod. Phys.* **A8**, 4755 (1993).
- [6] J. Bartels, *Z. Phys.* **C60**, 471 (1993) and further references therein.
- [7] S. Coleman and B. Grossman, *Nucl. Phys.* **B203**, 205 (1982); see also T. Banks, Y. Frishman, A. Schwimmer and S. Yankielowicz, *Nucl. Phys.* **B177**, 157 (1981).
- [8] V. N. Gribov, Orsay Lectures on Confinement (III), hep-ph/9905285.
- [9] A. A. Migdal, A. M. Polyakov and K. A. Ter-Martirosyan, *Zh. Eksp. Teor. Fiz.* **67**, 84 (1974); H. D. I. Abarbanel and J. B. Bronzan, *Phys. Rev.* **D9**, 2397 (1974).
- [10] A. R. White, hep-ph/0002303 - *The Past and Future of S-Matrix Theory in Scattering*, edited by E. R. Pike and P. Sabatier (to be published by Academic Press, London) and references therein.
- [11] P. Goddard and A. R. White, *Nucl. Phys.* **B17**, 1, 45 (1970). As in [3] we note that the full triple-regge limit is distinct from the “triple-regge” limit of the one-particle inclusive cross-section that is a “non-flip helicity-pole” limit.
- [12] O. Steinmann, *Helv. Phys. Acta.* **33** 257, 347 (1960); H. Epstein, in *Structural Analysis Of Collision Amplitudes* edited by R. Balian and D. Iagolnitzer (Amsterdam 1976), and references therein.